

# Intraseasonal to interannual variability of zooplankton biomass and standing stock inferred from ADCP backscatter in the eastern Arabian Sea

Ranjan Kumar Sahu<sup>a,b</sup>, D. Shankar<sup>a,b,\*</sup>, P. Amol<sup>b,c</sup>, S. G. Aparna<sup>a,b</sup>,  
D. V. Desai<sup>a,b</sup>

<sup>a</sup>*CSIR-National Institute of Oceanography, Dona Paula, 403004, Goa, India*

<sup>b</sup>*Academy of Scientific and Innovative Research (AcSIR), Ghaziabad, 201002,  
Uttar Pradesh, India*

<sup>c</sup>*CSIR-NIO Regional Centre, Visakhapatnam, 530017, Andhra Pradesh, India*

---

## Abstract

We analyse the variability of zooplankton biomass and standing stock (ZSS: integral of biomass over 24–120 m) at timescales ranging from intraseasonal to interannual using biomass data derived from seven ADCP (acoustic Doppler current profiler) moorings deployed on the continental slope in the eastern Arabian Sea (EAS) during 2017–2023. The biomass time series confirms the expected decay in biomass with depth. The monthly climatology of ZSS has its minimum (maximum) during the summer (winter) monsoon. The asymmetry reflected in the rapid rise (slow fall) in biomass following the minimum (maximum) leads to significant intra-annual (100–250 days) variability within the seasonal cycle. The annual cycle (300–400 days) dominates in the northeastern AS, but intra-annual and intraseasonal (5–90 days) variability dominate in the southeastern AS. The prominence of interannual variability is evident in the longer record. The intraseasonal range of biomass is comparable to or exceeds the seasonal range, but ZSS does not show com-

---

\*Corresponding author  
Email address: [shankar@nio.res.in](mailto:shankar@nio.res.in) (D. Shankar)

parable intraseasonal variability because the deviation from the mean can be in opposite directions in the upper and lower parts of the top  $\sim$ 140 m. Also evident are spikes that last a day or more and often exceed two standard deviations from the mean. The seasonal cycle and intraseasonal variability are not related to the variation of satellite chl-*a*, suggesting a significant role for the microbial loop and plankton not captured in satellite data. The strong intraseasonal variability calls into question biomass and ZSS contours based on traditional ship-based sampling.

*Keywords:* ADCP backscatter, moorings, zooplankton sampling, multiple plankton net, intraseasonal variability, Indian Ocean.

---

## 1. Introduction

### 2 1.1. Background

Zooplankton play a vital role in the pelagic ecosystem by enabling the  
4 hierarchical transport of organic matter from primary producers to higher  
trophic levels, thereby impacting the fish population (Ohman and Hirche,  
6 2001) and the carbon pump of the deep ocean (Quéré et al., 2016). Owing  
to their diel vertical migration (DVM), they probably constitute the largest  
8 migrating organism in terms of biomass (Hays, 2003). Zooplankton depend  
not only on phytoplankton, but also on the microbial loop (Azam et al.,  
10 1983); the zooplankton abundance or standing stock therefore depends on  
environmental variables (e. g., mixed-layer depth or MLD, insolation, oxy-  
12 gen, thermocline, nutrient availability, Chlorophyll-*a* (chl-*a*) concentration,  
and daily primary production). As is true of the rest of the world ocean,  
14 the biological productivity of the north Indian Ocean (NIO; north of 5°N  
in the Indian Ocean) is essentially driven by the physics and chemistry  
16 (see, for example, Subrahmanyam, 1959; Banse, 1968, 1995; Ryther et al., 1966; Nair, 1970; Qasim, 1977; Ba-  
18 , with changing dynamical conditions leading to variations in physico-chemical  
properties and therefore causing blooms and growth of plankton in favourable  
20 conditions. The changes are strongly influenced by the seasonal cycle in the  
NIO (Banse, 1968; McCreary et al., 1996, 2009; Lévy et al., 2007; Shankar  
22 et al., 2019; Aparna et al., 2022). The eastern boundary of the Arabian  
Sea contains the West India Coastal Current (WICC), which reverses sea-  
24 sonally, flowing poleward (equatorward) during November–February (June–  
September) (Banse, 1968; Shetye et al., 1990, 1991; Vijith et al., 2022; McCreary et al., 1993; Shankar  
26 et al., 1997; Shankar et al., 1997; Shetye et al., 1990, 1991; McCreary et al., 1993; Shankar and Shetye, 1997; Shankar et al., 1997).

28 A direct consequence of this reversal is the seasonal cycle of the thermocline (Shetye et al., 1990, 1991; Vijith et al., 2022) and oxycline (DeSousa et al., 1996; Schmidt et al., 2020) due to the upwelling (downwelling) favourable conditions during summer (winter) in the eastern Arabian Sea  
30 (EAS; Shetye et al., 1990, 1991; Vijith et al., 2022); the MLD responds to the changes in the thermocline and the mixing driven by the local winds and  
32 the changes in near-surface stratification (Shetye et al., 1991; Prasad and Bahulayan, 1996; Kumar and Narvekar, 2005). In response, the phytoplankton biomass and chl-*a* concentration changes with season (Subrahmanyam and Sarma, 1960; Banse, 1968; Kumar and Narvekar, 2005; Lévy et al.,  
34 2007; McCreary et al., 2009; Vijith et al., 2016; Shankar et al., 2019). Upwelling during the summer monsoon leads to maximum chl-*a* growth in the  
36 EAS (Banse, 1968; Banse and English, 2000; McCreary et al., 2009; Hood et al., 2017; Bemal et al., 2018; Shi and Wang, 2022). During the winter monsoon, convective mixing driven by dry winds was considered the key process leading to the deep mixed layer in the northeastern Arabian Sea  
38 (NEAS; Banse, 1968; Shetye et al., 1992; Madhupratap et al., 1996b; McCreary et al., 1996; Lévy et al., 2007), but recent results show that the poleward advection of warm and fresher water plays a key role in restricting the  
40 deep mixed layers to the northern part of the NEAS (Shankar et al., 2016).  
42 This deepening of the mixed layer leads to a winter chl-*a* peak in the NEAS  
44 (~~Madhupratap et al., 1996b; McCreary et al., 1996; Lévy et al., 2007; Shankar et al., 2016; Vijith et al., 2016~~)  
46 (Madhupratap et al., 1996b; McCreary et al., 1996; Lévy et al., 2007; Vijith et al., 2016; Shankar et al., 2016).  
48 In the southeastern Arabian Sea (SEAS), downwelling Rossby waves modulate chl-*a* during the winter monsoon, but this effect is limited to the neighbourhood of the coast and islands (Amol et al., 2020); hence, the chl-*a*  
50 .

54 peak in the SEAS is limited to the summer monsoon.

The zooplankton grazing peak is instantaneous with no time delay from  
55 peak phytoplankton production (Li et al., 2000; Barber et al., 2001), but its  
population growth lags (Rehim and Imran, 2012; Almén and Tamelander,  
56 2020) depending on its gestation period and other limiting aspects. Some  
studies suggest that the peak timing of zooplankton may not change in par-  
58 allel with phytoplankton blooms (Winder and Schindler, 2004), but others  
indicate that a lag exists between primary production and the transfer of en-  
60 ergy to higher trophic levels (Brock and McClain, 1992; Brock et al., 1991).  
Conventional, ship-based zooplankton sampling, by capturing only a few  
62 snapshots of the variation, provides an incoherent or incomplete description  
of the spatio-temporal variation of zooplankton (Ramamurthy, 1965; Mad-  
64 hupratap et al., 1992; Piontkovski et al., 1995; Madhupratap et al., 1996a;  
Wishner et al., 1998; Nair et al., 1999; Barber et al., 2001; Jyothibabu et al.,  
66 2010; Khandagale et al., 2022). Generating a time series of zooplankton  
biomass and standing stock is, however, possible with calibrated acoustic  
68 instruments such as the acoustic Doppler current profiler (ADCP) (Edvard-  
sen et al., 2003; Smith and Madhupratap, 2005; Smeti et al., 2015; Kang  
70 et al., 2024). The ADCP, by providing a continuous time series at a high  
72 temporal resolution, can reveal details of the complex interplay between the  
74 physico-chemical and ecosystem variables (Jiang et al., 2007; Potiris et al.,  
2018; Shankar et al., 2019; Aparna et al., 2022; Nie et al., 2023), and has  
76 been used to map zooplankton migration (Inoue et al., 2016; Ursella et al.,  
2018, 2021) and their seasonal to annual variation (Jiang et al., 2007; Hobbs  
78 et al., 2021; Liu et al., 2022; Aparna et al., 2022).

The relationship between ADCP backscatter and the abundance and  
80 size of zooplankton was described by Greenlaw (1979) with mono-frequency

backscatter used to estimate abundance along with knowledge of mean zooplankton size. The popularity of the ADCP as a tool to study temporal and spatial variation of zooplankton biomass increased in the 1990s following the introduction of high-frequency echo sounders (Flagg and Smith, 1989; Wiebe et al., 1990; Batchelder et al., 1995; Greene et al., 1998; Rippeth and Simpson, 1998). The ADCP backscatter has been used to study DVM and the spatial and temporal variability of zooplankton biomass in different marine regions, such as the southwestern Pacific (Smeti et al., 2015), the Lazarev Sea in Antarctica (Cisewski et al., 2010), the Canadian Arctic (Hamilton et al., 2013), and the Corsica Channel in the northwestern Mediterranean Sea (Guerra et al., 2019). Yet, in spite of the existence of moored-buoy networks deployed across the world ocean to measure currents, the potential of acoustics for understanding coupled physical and biological processes is poorly exploited (Davis et al., 2019; Shankar et al., 2019; Aparna et al., 2022). Aparna et al. (2022) (A22 hereafter) showed how the ADCP mooring network in the EAS (Amol et al., 2014; Chaudhuri et al., 2020) could be used to map the seasonal cycle of zooplankton biomass and standing stock, permitting an analysis of the physico-chemical forcing of their climatological seasonal variation.

### 100    1.2. Objectives and scope

The network of ADCPs used by A22 to map the seasonal cycle of zooplankton biomass and standing stock was originally deployed on the continental slope off the west coast of India to map the variability of the WICC on time scales ranging from the seasonal to the intraseasonal and to provide a measure of its interannual variability (Amol et al., 2014; Chaudhuri et al., 2020). A22 showed that the zooplankton peaks (and troughs) are influenced

by the seasonal movement of the thermocline, the oxygen minimum zone  
108 (OMZ), and the MLD. Their analysis showed that the zooplankton standing stock (ZSS) tends to decrease in the SEAS during the summer monsoon,  
110 when upwelling facilitates an increase in phytoplankton biomass.

A22 used ADCP backscatter data from three moorings, one each located  
112 off Mumbai (NEAS), Goa (central-eastern Arabian Sea or CEAS), and Kollam (SEAS) for the period October 2012 to December 2020. We extend  
114 the work of A22 by presenting data from four additional moorings in the EAS and highlight the significant intraseasonal variability of biomass and  
116 ~~standing stock ZSS~~ revealed by the ADCP data. The article is organized as follows: data sets and methods employed are described in Section 2. Section 3 describes the observed time series and the climatology of zooplankton biomass and ~~standing stock ZSS~~, and their seasonal cycle and variability.  
120 A brief discussion on interannual variability in Section 4 is followed by a detailed discussion in Section 5 on intraseasonal variability, which is a major focus in this study. Section 6 summarises the results and discusses their implications.  
122

## 124 2. Data and methods

In this section, we describe the data sets used in this article: the primary data ~~are consist of~~ ADCP backscatter (Section 2.1) and zooplankton biomass (Section 2.2), ~~but we also use other along with additional supporting~~ data sets (Section 2.3). ~~A detailed description of the time series analysis methods—such as wavelet analysis (Torrence and Compo, 1998; Maraun and Kurths, 2004)~~  
126 ~~implemented using the PyCWT module, and filtering using the Lanczos filter, is provided in supplementary Section XX.~~  
128  
130

132    2.1. *The ADCP backscatter time series*

The ADCP backscatter forms the primary data set used in this article.

134    The four additional moorings include one off Kanyakumari (in the SEAS,  
135    south of Kollam and on the slope off the southern tip of the Indian main-  
136    land), Udupi (just north of the SEAS–CEAS boundary), Jaigarh (north of  
137    Goa in the CEAS), and Okha (north of Mumbai in the NEAS); all these  
138    mooring locations are shown in Fig. 1 and listed in Table 1. The AD-  
139    CPs are of make Teledyne RD Instruments, upward-looking, and operate at  
140    153.3 kHz. Though the Kanyakumari mooring had been deployed in 2009,  
141    the top ADCP had a frequency of 76.8 kHz till January 2016, over two  
142    years after the shift to 153.3 kHz off Kollam, Goa, and Mumbai (Chaudhuri  
143    et al., 2020). That’s why the Kanyakumari mooring was not included in  
144    the analysis of A22. We include it in our analysis because the 153.3 kHz  
145    measurements started in October 2017, when the ~~other~~additional three  
146    moorings were deployed in the EAS. The ADCP data used herein span the  
147    period October 2017 to December 2023, but there are data gaps at some  
148    locations (Table 1).

The moorings on the west-coast slope are serviced once a year during

150    September–December depending on ship availability. Data was collected at  
151    hourly intervals with a 4 m bin size. The echoes at the surface render the  
152    data useless within roughly 10% of the transducer’s range ( $\sim$ 20 m) and this  
153    data is therefore discarded. We have followed the methodology laid down in  
154    A22 to derive the backscatter time series from ADCP echo intensity. Gaps  
155    up to two days are filled using the grafting method of Mukhopadhyay et al.  
156    (2017) and the graft-filled backscatter time series is converted to zooplankton  
157    biomass.

158    Off Kanyakumari, the top ADCP landed at a depth of  $\sim$ 300 m in the

last deployment in January 2023 and backscatter data are not available in  
160 the top  $\sim$ 120 m, precluding use of this record. Off Jaigarh, only a 76.8 kHz  
ADCP could be deployed at the top; while this frequency does not matter  
162 for the currents, it does matter for the backscatter, and the data from this  
deployment is not used. Off Okha, data is not available for the entire upper  
164  $\sim$ 120 m for the second deployment (2018–2019).

## 2.2. The zooplankton biomass time series

166 In situ biomass data from volumetric zooplankton samples are used to  
convert the backscatter to biomass. The zooplankton samples were collected  
168 in the vicinity ( $\sim$ 10 km) of the ADCP mooring site twice, once prior to re-  
trieval and again following the deployment of the mooring (Table 2). A  
170 multi-plankton net (MPN, 100  $\mu$ m mesh size, 0.5~~x~~<sup>0.5</sup> m<sup>2</sup> mouth area) was  
used to collect samples over pre-determined depth ranges; the water volume  
172 filtered was calculated by sampling depth range and mouth area. The timing  
of sample collection was different throughout the MPN hauls owing to its  
174 dependence on the time ~~or of~~ mooring retrieval, but ~~from 2020 onward,~~ the  
depth range was standardized ~~from 2020 onwards to the bins over to fixed~~  
176 ~~depth ranges of~~ 0–25, 25–50, 50–75, 75–100, and 100–150 m. Following nu-  
merous previous studies (A22; Flagg and Smith, 1989; Heywood et al., 1991;  
178 Jiang et al., 2007), the backscatter was averaged in the vertical correspond-  
ing to the specific ~~bins depth range~~ of the MPN haul for each site, and then  
180 linearly regressed with the biomass of ~~respective bins corresponding depth~~  
~~range~~ (Fig. 2). The zooplankton biomass in the euphotic zone concentrates  
182 in the upper 10 m and this shift to near the surface is pronounced during  
the night. Yet, this should not be a concern for the regression as it would  
184 simply show up as low backscatter at deeper depths during night-time cor-

responding to low biomass. It is important to note that the study is carried  
186 out using daily averaged biomass. Therefore, features associated with the  
DVM are eliminated (A22; Jiang et al., 2007).

188 The zooplankton biomass time series (Fig. 3) is created from the above  
linear regression. ~~The standing stock ZSS~~ is determined by taking the ver-  
190 tical integral of biomass over the water column. ~~As in Following~~ A22,  
to ~~maintain consistency in the estimation of standing stock over ensure~~  
192 ~~consistency in ZSS estimation across~~ the time series, only those deployments  
~~that do not lack data at any depth in the entire with complete data coverage~~  
194 ~~throughout the full depth~~ range of 24–120 m are considered for analysis. ~~The~~  
m were included in the analysis. ~~For a few years, the~~ lack of data above  
196 ~~~24~~<sup>140</sup> m is due to the deviation in the vertical position of the ADCP  
transducer in the water column. In spite of the care taken to position the  
198 instrument (mooring) at ~150–200 m (~1050–1100 m) depth, the process  
of mooring deployment, which is done from a steaming ship, implies that  
200 some deployments are shallower or deeper owing to drift caused by floater-  
buoyancy and anchor-weight imbalance. It leads to a gap in the data at some  
202 mooring sites for some years. For example, off Okha, data is not available  
for the entire upper 120 m depth for the second deployment (2018–2019).  
204 Data is also unavailable off Jaigarh from the surface to ~60 m data during  
206 2019–2022 and off Kollam below ~80 m during 2020–2021. There are also  
a few deployments during which no data or bad data was recorded, e. g,  
off Udupi (2020–2021) and Kanyakumari (2022–2023); such bad data are  
208 discarded from standing-stock estimation.

A decrease in biomass with increasing depth is observed at all seven  
210 locations (Fig. 3). To demarcate this expected decrease in biomass from the  
more productive upper ocean to the less productive lower ocean, A22 used

the 215 mg m<sup>-3</sup> biomass contour (called  $z_{215}$ ), and this contour is plotted for both daily and monthly time series in Fig. 3; the depth of this contour is called  $D_{215}$ . The lower biomass in the upper ocean off Kanyakumari and Okha, however, led us to use the 175 mg m<sup>-3</sup> for these locations. This contour, whether  $D_{215}$  or  $D_{175}$ , cannot be plotted when data are missing, leading to some gaps in its time series.

The biomass decrease with depth, roughly defined as the difference between mean biomass at 40 m and 104 m, is highest off Jaigarh and Mumbai, owing to the higher biomass in the upper ocean and lowest off Kanyakumari (Fig. 4, Table S2); this biomass decrease in the vertical is comparable at the other four locations. (A22 had reported that the decrease in biomass was lower off Kollam compared to Mumbai and Goa.)  $D_{215}$ , like the biomass at 40 m or 104 m, shows a seasonal variation: it moves up during the summer monsoon, when upwelling occurs, and down during the winter monsoon, when downwelling occurs. Note, however, that there is striking variation in  $D_{215}$  over the years sampled: indeed, the high difference between 40 m and 104 m is due to a few years rather than being a standard feature of the entire record at a given location (Figs. 3,4). The mean and standard deviation of biomass are shown in Table S2. The sites with higher biomass tend to have higher variation over time, e. g., Mumbai, Jaigarh, and Kollam.

### 2.3. Other data sets

We also use data on temperature, salinity, MLD, oxygen, chl-*a* and satellite-derived sea-level anomalies (SLAs).

As in A22, in order to compare the changes in ZSS with the vertical movement of the thermocline, we use the monthly temperature climatology of Chatterjee et al. (2012) (1° spatial resolution); the depth of the 23°C

238 isotherm (henceforth,  $D_{23}$ ) is used as a proxy for the thermocline. Following  
A22, for comparison with the vertical movement of the oxycline, we use the  
240 monthly climatology of oxygen from the World Ocean Atlas 2013 (García  
et al., 2014). The oxygen concentration contour used as a proxy for the  
242 oxycline is specific to each site owing to the presence of some locations  
within the OMZ and some locations outside its boundaries in the EAS.  
244 We use  $2.1 \text{ ml L}^{-1}$  for Kanyakumari and Kollam,  $3.2 \text{ ml L}^{-1}$  for Okha,  
and  $1.7 \text{ ml L}^{-1}$  for the other four locations; Kanyakumari, Kollam, and  
246 Okha lie outside the core of the OMZ in the EAS (see Fig. 1), but Okha  
is ventilated better owing to the intrusion of the Arabian Sea High Salinity  
248 Water (ASHSW; Rochford, 1964; Wyrtki et al., 1971) from farther north  
in the NEAS (Banse and Postel, 2009; Naqvi et al., 2006; Shankar et al.,  
250 2016). The MLD in the EAS is of the order of  $\sim 20\text{--}40 \text{ m}$  during the summer  
monsoon (Shetye et al., 1990; Shankar et al., 2005; Sreenivas et al., 2008),  
252 especially in the SEAS (Shenoi et al., 2005), but the MLD remains deep in  
the northern NEAS during winter (Shankar et al., 2016). As in A22, the  
254 climatological MLD is calculated using the temperature and salinity from  
the Chatterjee et al. (2012) data set using a density criterion: the MLD is  
256 defined as the depth at which the density increase from the surface **surface**  
corresponds to a  $0.5^\circ\text{C}$  decrease in temperature (Shenoi et al., 2004).

258 A22 used chl- $a$  data from SeaWiFS, but this satellite ended service in  
260 2010; A22 could still use this data set because their use of chl- $a$  was limited  
to a climatology. Since we want a time series of chl- $a$ , we use the new  
262 chl- $a$  product from Global Ocean Colour. Biogeochemical Level-4 data is  
obtained from E. U. Copernicus Marine Service Information. The daily  
264 data is available at a spatial resolution of 4 km, but, like all satellite chl- $a$   
data, has gaps due to clouds. Hence, to ensure a continuous time series,

after applying the grafting method of Mukhopadhyay et al. (2017) on chl-*a*  
266 a trade-off is made between minimising the gaps in chl-*a* data and retention  
of at least 10 data points for computing the 30-day running-mean.

268 A22 used the depth of the 20°C isotherm, estimated from the climatology  
of Chatterjee et al. (2012), as a measure of the physical forcing (essentially  
270 upwelling or the vertical movement of the thermocline). Since this variable  
is not available as a time series, we use the satellite-derived SLA as a  
272 proxy for the thermocline. The SLA data (daily L4 data on a 0.25° × 0.25°  
grid) was extracted for the period of interest (October 2017 to December  
274 2023) from E. U. Copernicus Marine Service Information.

### 3. The seasonal cycle

276 In this section, we discuss the seasonal climatology and the seasonal cycle  
in the time series.

#### 278 3.1. Climatology of zooplankton biomass and standing stock

The monthly climatology of biomass, ZSS, and chl-*a* was computed from  
280 the monthly means, which were estimated for every month for which at least  
10 days of data were available. Therefore, since we have used all the available  
282 data at each location, the number of years for which the average is computed  
is not the same at all locations because there are some gaps at some locations  
284 (Okha, for example). Yet, the similar behaviour of the A22 climatology  
(2012–2020) and our climatology (2018–2022) off Kollam, Goa, and Mumbai  
286 (see Section S1) suggests that the basic features are strong aspects of the  
seasonal climatology. Such strong features include the following (Fig. S1):  
288 the decrease in zooplankton biomass from the upper ocean to below *D*215 is  
weaker off Kollam compared to Goa and Mumbai; there is high ZSS during

290 the winter monsoon at all three locations in the EAS; there is a mismatch  
291 in the chl-*a* peak, which occurs during the summer monsoon, and the ZSS  
292 peak, which occurs during the winter monsoon, off Kollam. While some  
293 other details may vary between the two climatologies (higher zooplankton  
294 biomass off Kollam and lower biomass off Goa in the new climatology), the  
295 basic features are consistent. We can infer that phytoplankton dominate  
296 in the SEAS and the microbial loop in the NEAS, a conclusion reached  
297 by both A22 and Shankar et al. (2019), which allowed the latter to infer  
298 explain why planktivorous (carnivorous) fish like the oil sardine (Bombay  
Duck) dominate in the SEAS (NEAS).

300 The four additional moorings throw more light on this transition from  
301 a phytoplankton-dominated ecosystem in the SEAS to a microbial-loop-  
302 dominated ecosystem in the NEAS. We find a decrease in the mean chl-*a*  
303 from Kollam ( $0.58 \text{ mg m}^{-3}$ ) to Jaigarh ( $0.28 \text{ mg m}^{-3}$ ), and an increase  
304 farther north in the NEAS (Fig. 5, Table S1). The change in the range  
305 or standard deviation (SD) of chl-*a* is, however, much more striking from  
306 Kollam to Okha: the range decreases from  $2.32 \text{ mg m}^{-3}$  off Kollam to just  
307  $0.24 \text{ mg m}^{-3}$  off Goa, before increasing again to  $0.7 \text{ mg m}^{-3}$  off Okha.  
308 Therefore, chl-*a* and the range of its variation are weaker in the CEAS  
309 and increase on either side of Jaigarh. The variation of ZSS is in striking  
310 contrast that of chl-*a*. The mean ZSS decreases from Kollam ( $24.6 \text{ g m}^{-2}$ )  
311 to Goa ( $21.2 \text{ mg m}^{-2}$ ), but increases to  $24.2 \text{ g m}^{-2}$  (practically the same  
312 as off Kollam) off Jaigarh before decreasing farther north. The range of  
313 ZSS variation, however, increases over twofold from  $4.1 \text{ g m}^{-2}$  off Kollam to  
314  $9 \text{ g m}^{-2}$  off Jaigarh before decreasing again farther north. So the conclusion  
315 of a phytoplankton-dominated (microbial-loop-dominated) ecosystem in the  
SEAS (NEAS) inferred by A22 is strengthened by the new climatology:

the transition tends to occur in the CEAS and can be considered to occur  
318 roughly north of Udupi owing to the significant decrease in the range of chl-*a*  
from Udupi to Goa.

320 The mooring location off Kanyakumari is distinct from the other six  
mooring locations because the former lies at the junction of the Bay of Ben-  
322 gal and the Arabian Sea, in the regime of the seasonally reversing monsoon-  
current system (Shankar et al., 2002); the other six moorings lie on the  
324 slope off the Indian west coast. Therefore, we excluded Kanyakumari from  
the above discussion of chl-*a* and ZSS variation along the west-coast slope.  
326 This change in location *vis-a-vis* the west coast is seen in the chl-*a* and ZSS  
variation off Kanyakumari, where we find a high range of chl-*a* about a high  
328 mean chl-*a*, while the ZSS shows a low range of variation about a low mean  
(Fig. 5, Table S1). Off Jaigarh, in contrast, we find a high range of ZSS and  
330 a negligible range of chl-*a* about a low mean chl-*a*.

### 3.2. Seasonal cycle and variability

332 This seasonal cycle is evident in the time series (Fig. 4) and in the wavelet  
power spectra (see Section S2.[1](#) for a brief discussion of wavelet analysis) of  
334 the biomass at 40 m and 140 m (Fig. 6) and the ZSS (Fig. 7). It is also  
seen in the biomass filtered in the seasonal band (see Section S2.[2](#) for a brief  
336 discussion of filtering) of 100–400 days (Fig. 8) to extract only the seasonal  
variability, i. e., variability at a period of over three months so that it can  
338 be captured to an extent in a monthly time series. The wavelet spectra  
of biomass (Fig. 6) show high variability, denoted by the reddish colours,  
340 at all locations, but the strength of this variability is not the same. Off  
Kanyakumari, for example, the variability in the seasonal band is low, as  
342 indicated by the colour at both depths; in contrast, the seasonal variability

appears strong in the wavelet spectra off Goa and Mumbai. In the filtered  
344 plot (Fig. 8), this change from Kanyakumari to Jaigarh is seen in the weaker  
shades of red and blue off Kanyakumari compared to the deeper shades off  
346 Jaigarh. The utility of the wavelet spectrum and the filtered biomass lies,  
however, in their ability to show how this seasonal variability, indicated by  
348 the wavelet power or the colour shade, changes over time. For example, the  
change in shades shows that the seasonal cycle is weak in both the wavelet  
350 spectrum of biomass at 40 m and the filtered biomass off Kollam during  
2020 and increases from 2021 onwards off Goa.

352 Note also that the colour often switches in the filtered plot from red  
(positive deviation from the mean) to blue (negative deviation from the  
354 mean) around  $D175$  or  $D215$  (Fig. 8), which are defined using the monthly  
time series of biomass, pointing to the role of this contour in separating  
356 the upper and lower ocean with respect to the zooplankton biomass. When  
such a change of colour occurs, the positive and negative deviations on either  
358 side of the curve cancel each other in the vertical integral to determine ZSS.  
this behaviour occurs over timescales ranging from intraseasonal to annual  
360 ([Fig. S3](#)). Hence, since such a change across  $D175$  is seen frequently off  
Kanyakumari, the ZSS at this location shows a negligible variation, leading  
362 to a low SD in the climatology (Fig. 5, Table S1, [Fig. S3](#)) and over the time  
series (Table S4). The SD increases in the CEAS, but decreases again in the  
364 NEAS (Table S4).

Another feature noted by A22 and striking in the climatological ZSS  
366 (Fig. 5) is the asymmetry in time: the increase from the minimum dur-  
ing the summer monsoon occurs much faster than the decrease from the  
368 maximum during the winter monsoon. This asymmetry, which is more pro-  
nounced in the NEAS and CEAS (Fig. 5, Table S1), is a consequence of the

370 temporal asymmetry in the monsoon winds and the resulting asymmetry  
in the ~~circulation~~ circulation (see, for example, Shankar et al., 2002, 2019):  
372 this variability has been noted earlier in the west-coast alongshore currents  
(Amol et al., 2014; Chaudhuri et al., 2020). As a result, there is significant  
374 variability at the semi-annual period ( $\sim$ 180 days) in addition to the annual  
period ( $\sim$ 365 days). Amol et al. (2014) split the seasonal variability of the  
376 current in the 100–400-day period band (~~see Section S2~~) into two distinct  
bands, the annual band in the period range 300–400 days and the intra-  
378 annual band in the period range 100–250 days. The wavelet spectra show  
that the variability in the intra-annual band of  $\sim$ 100–250 days is not con-  
380 fined to the semi-annual period of 180 days, but extends to lower periods  
within this band. In the currents, variability around  $\sim$ 120 days has been  
382 noted (Amol et al., 2014; Chaudhuri et al., 2020), and variability around this  
period is also seen in the biomass (Fig. 6) at some locations. For example, off  
384 Kollam, the wavelet spectrum at 40 m shows variability around  $\sim$ 180 days  
in 2019–2020, but it is stronger at lower periods within this intra-annual  
386 band in 2021–2022. In general, the annual band for zooplankton biomass  
tends to be weaker than the intra-annual band (Figs. 6,S2, Table S3). Even  
388 within the weak seasonal cycle off Kanyakumari, variability is stronger in  
the intra-annual band compared to the annual band (Fig. S2, Table S3).

390 **4. Interannual variability**

Interannual variability of the monthly time series may be considered to  
392 occur in two ways. First, there can be years in which the biomass or ZSS  
changes in one direction throughout the year, implying a significant devia-  
394 tion from the seasonal cycle, but at a period clearly different from variability

within a season. Second, there can be a variability that is captured at a period higher than a year in a Fast Fourier Transform (FFT) or a wavelet spectrum.

The first kind of interannual variability is obvious from a comparison of the biomass climatology (Fig. 5) and the biomass time series (Fig. 3). It is clear, for example, that the high climatological biomass above  $D215$  off Kollam during the summer monsoon is due to the high biomass occurring during a few years: the red colour, implying high wavelet power, is seen in 2022 and to a lesser extent in 2021 and 2022, but it is missing in earlier years. A more striking case occurs during 2020, when the biomass off Kollam collapsed over the entire depth range of sampling (Fig. 3; see Section S3) and this lower biomass is clearly seen in the biomass curves at 40 m and 140 m (Fig. 4). A consequence of this collapse in zooplankton biomass is the significantly lower ZSS during 2020 off Kollam (Fig. 4). Such deviations, but usually of a weaker magnitude, from the expectation of the seasonal climatology occur fairly frequently at all locations. Off Goa, the climatology of A22 shows higher biomass above  $D215$  than does the new climatology (Fig. S1); an examination of the data for 2012–2020 shows lower biomass during the summer monsoon in most of the years sampled in the new climatology compared to that of A22, leading to lower power around the annual band ( $\sim 360$  days) in the wavelet spectrum in the second half of the record (Fig. 9).

The second kind of interannual variability requires a change that occurs over more than a year. A22 noted the presence of this second kind of interannual variability off Kollam: the wavelet spectrum showed high power in a band around 720 days or roughly two years, but it was outside the wavelet cone of influence (see Section S2), implying that the time series was too short

<sup>422</sup> for the seeming quasi-biennial oscillation (QBO; Mooley and Parthasarathy,  
<sup>424</sup> 1984; Bhalme et al., 1987), a well-known signal in Indian monsoon rainfall  
<sup>426</sup> and therefore of monsoon variability, to be statistically significant. The per-  
sistent signal did, however, suggest a longer record would prove its existence  
<sup>428</sup> off Kollam. An examination of the wavelet spectrum over 2012–2022 shows  
a strong signal at this period during 2012–2018 (Fig. 9), but it weakens af-  
<sup>430</sup> ter that and the interannual band seems to shift to higher periods (Fig. 9).  
The QBO signal is also seen off Mumbai in the middle of the record, but  
<sup>432</sup> appears at a higher period before 2017 and after 2021; it is weaker off Goa  
and appears outside the cone of influence (Fig. 9).

## <sup>432</sup> 5. Intraseasonal variability

Apart from interannual variability, A22 also commented on the exis-  
<sup>434</sup> tence of intraseasonal variability in the daily biomass data obtained from  
the ADCP backscatter. Though they did not analyse it, A22 pointed out  
<sup>436</sup> that this variability within a season is not small.

### 5.1. The wavelet spectrum

<sup>438</sup> That this intraseasonal variability is strong is clearly seen in the devia-  
tion of the light-coloured curves for the daily data from the darker curves for  
<sup>440</sup> the 30-day running mean of the biomass at 40 m and 104 m, and in the ZSS  
(Fig. 4). These significant deviations lead to a clear signal in the wavelet  
<sup>442</sup> power at periods below 90 days for the 40 m and 104 m biomass (Fig. 6).  
Unlike the wavelet power at the seasonal time scales, which tends to be  
<sup>444</sup> continuous in, say, the annual band for a year or more, the intraseasonal  
wavelet power is patchy, as has been seen earlier for the currents (Amol  
<sup>446</sup> et al., 2014; Mukherjee et al., 2014; Chaudhuri et al., 2020; Mukhopadhyay

et al., 2020). This patchiness is a consequence of the intraseasonal biomass  
448 bursts not occurring throughout the year or the time series, but on occasions  
within a season. The intraseasonal variability is prominent in the 30–90-day  
450 band in the wavelet power spectrum, but there is also variability at peri-  
ods shorter than 30 days (Fig. 6). For the currents, the lower bound used  
452 was  $\sim$ 5 days in order to filter out inertial currents off Kanyakumari, which  
has the highest inertial period of the seven locations (Amol et al., 2014;  
454 Chaudhuri et al., 2020). We retain this lower limit for our analysis of the in-  
traseasonal variability of biomass and ZSS, i. e., we define the intraseasonal  
456 variability to occur in the period range of 5–90 days, with the 30–90-day  
(5–30-day) band constituting the “low-frequency” (“high-frequency”) parts  
458 of the intraseasonal spectrum; the low-frequency part of this band is marked  
by the horizontal lines in the wavelet plots.

460 The wavelet power is not normalised in this analysis. Therefore, even if  
the amplitude is the same at two different periods, the wavelet power will  
462 be less for the higher frequency ([https://paos.colorado.edu/research/  
wavelets/faq.html](https://paos.colorado.edu/research/wavelets/faq.html)). Hence, we cannot infer from the red (yellow) colours  
464 for the seasonal (intraseasonal) band in the wavelet spectrum (Fig. 6) that  
variability is higher in the seasonal band. Though this limitation of the  
466 wavelet spectrum can be overcome by normalising the wavelet power, we  
prefer to apply band-pass filters to extract the variability in the intraseasonal  
468 band (Fig. 10), as done earlier for the seasonal cycle (Fig. 8), because the  
result of this filtering is more intuitive.

470 *5.2. Range of intraseasonal variability*

Filtering the biomass with a band-pass filter (Fig. 10) suggests that the  
472 biomass range in the 5–90-day or intraseasonal band is comparable to that

in the seasonal band (Fig. 8) and it often exceeds the seasonal range. (As  
474 noted earlier for the filtered plot of the seasonal cycle, the filtered intrasea-  
sonal biomass shows the deviation from the mean, leading to both positive  
476 (red) and negative (blue) values.) The short time scale associated with the  
intraseasonal band makes it difficult to draw inferences from a plot of the  
478 entire time series (Fig. 10); hence, we present the analysis for 2019. This  
year is chosen because this deployment was not at the beginning or end of  
480 the time series (See Section S2 for the impact of filtering at the ends of  
the time series.) and there are fewer data gaps in the daily biomass time  
482 series. Note that our interest here is limited to showing that there is strong  
intraseasonal variability in zooplankton biomass, not in the details of this  
484 variability for any year (including 2019). Hence, we show only the Kollam  
figure for 2019 here (Fig. 11); the figures for the other locations are available  
486 in the supplement (Figs. S4–S9).

The expanded time axis shows that the range of biomass at 40 m in the 5–  
488 90-day band (Fig. 11b) is comparable to that in the seasonal band (Fig. 11a)  
off Kollam. There are, however, significant periods when intraseasonal vari-  
490 ability is weak (lighter shades of blue and red in Fig. 11b); these relatively  
quiescent periods are compensated by the occasions on which the intrasea-  
492 sonal range is significantly higher than the seasonal range (Fig. 11a,b,c). The  
daily biomass at 40 m is therefore determined by significant contributions  
494 from both seasonal and intraseasonal bands, with the relative contributions  
changing through the year: strong intraseasonal bursts lasting roughly a  
496 month are seen from the end of July through October (Fig. 11c). This re-  
sult, that the range of intraseasonal variability is comparable to the seasonal  
498 range, is also true for the rest of the time series off Kollam (Figs. 8,10), lead-  
ing to the SD for both bands being comparable at 40 m (Table S3). The

same comparison holds off Udupi (Figs. 10,S5, Table S3), which lies just north of the boundary between the SEAS and the CEAS. Off Kanyakumari, however, the significantly weaker seasonal cycle (Fig. 8) leads to a higher range (Fig. S4) and SD (Table S3) for the intraseasonal band. The higher range of the intraseasonal band is also evident off Goa (Fig. S6) and Jaigarh (Fig. S7) in the CEAS (Fig. 10, Table S3). A stronger seasonal cycle at NEAS compared to the CEAS implies that range of the seasonal and intraseasonal bands is again comparable off Mumbai (Fig. S8, Table S3). Off Okha, the data gaps imply that the filled part of the seasonal band is small (Fig. 8); hence, it is difficult to attach much significance to the higher intraseasonal range indicated by the high SD in this band (Table S3).

At 104 m, i. e., below  $D215$  or  $D175$ , the range of the intraseasonal band is less than at 40 m off Kanyakumari (Fig. S4c), Kollam (Fig. 11c), and Udupi (Fig. S5c), i. e., in the SEAS (Table S3). The range at both depths is comparable at the other locations. The intraseasonal range is higher than the seasonal range off Kanyakumari and Jaigarh, lower than the seasonal range off Udupi, and of a similar magnitude at the other locations, including Kollam (Figs. 8,10,11,S4–S9, Table S3). Therefore, even the non-monotonic pattern for the intraseasonal range that is suggested by the data at 40 m is not applicable at 104 m.

### 520 5.3. Spikes in biomass

Striking at both 40 m and 104 m, however, is the seemingly higher range of the daily biomass than is indicated by an addition of the biomass in the seasonal and intraseasonal bands (Figs. 11c,S4c–S9c). Part of this difference may be due to interannual variability, i. e., biomass varying at periods higher than  $\sim 400$  days. Therefore, we applied a 5-day low-pass filter to the biomass

526 to include this variability at time scales longer than the seasonal, and com-  
527 pared the resulting curve with the daily biomass (Figs. 11d,S4d–S9d). The  
528 two curves almost overlap, suggesting that almost the entire variability of  
529 the daily biomass curve at any depth can be explained by adding the vari-  
530 ability in the intraseasonal, seasonal, and interannual bands. The slight  
531 difference between the black and red curves (blue and cyan curves) for the  
532 low-passed and daily biomass at 40 m (104 m) suggests, however, that there  
533 is some variability at periods shorter than 5 days. An example of such a  
534 difference at 40 m occurs towards the end of July off Kollam (Fig. 11d).

Subtracting the 5-day low-passed biomass from the daily biomass shows  
535 the existence of spikes in the daily biomass (Figs. 11e,S4e–S9e). On several  
536 occasions, these spikes exceed one SD (dark grey background) and they  
537 exceed two SD (light grey background) on a few occasions. Examples of  
538 spikes exceeding two SD at 40 m are seen towards the end of July and  
539 August and in September off Kollam (Figs. 11e,[S10](#)[S11](#)). Similar spikes are  
540 seen in the biomass at 104 m, but fewer of these spikes exceed one SD or  
541 two SD: one spike exceeding two SD occurs in the last week of October off  
542 Kollam (Fig. [S11](#)[S12](#)). Such spikes, which extend the peaks in the daily  
543 biomass above the sum of the seasonal and intraseasonal bands, are also  
544 evident at the other six locations (Figs.S4e–S9e); the largest spikes occur off  
545 Jaigarh (Fig. S7e) at both 40 m (Fig. [S10](#)[S11](#)) and 104 m (Fig. [S11](#)[S12](#)).

These spikes, particularly in comparison to one SD, occur at random  
546 throughout the year. The positive spikes are caused by an increase in the  
547 biomass over a day or a few days, with lower biomass on either side of this  
548 increase. The negative spikes are caused by a decrease in biomass with  
549 respect to the [higher](#) biomass before and after this spike.

552    5.4. Variation in standing stock

The ZSS is obtained by integrating the biomass in the vertical, implying  
554 contributions from both above and below  $D215$  or  $D175$ . The mean biomass  
is considerably less below this contour (Table S2), but the variability about  
556 this mean also matters. In the SEAS (Kanyakumari and Kollam), both  
seasonal and intraseasonal SD are much higher at 40 m (Table S3). Off  
558 Udupi, the seasonal range is comparable at these depths, but the intrasea-  
sonal range is high, as in the SEAS. The CEAS emerges as a regime where  
560 changes occur. Off Goa, the seasonal and intraseasonal ranges are compa-  
rable at these depths, but the behaviour is different off Jaigarh, where the  
562 intraseasonal ranges are comparable even though the seasonal range is much  
less at 40 m. In the NEAS, both seasonal and intraseasonal ranges are com-  
parable. (Note that the seasonal range off Okha is based on a short record.)  
There are occasions when high variability in the 30–90-day band is seen at  
566 both depths in the wavelet spectrum (Fig. 6) and in the filtered biomass  
(Fig. 10); an example is during August–November 2018 off Udupi, Goa, and  
568 Jaigarh in the CEAS. Variability in this band is also seen off Kollam and  
Mumbai during August–November 2018, but it is clearly weaker and more  
570 short-lived (Figs. 6,10).

In both bands, seasonal (Fig. 8) or intraseasonal (Figs. 10,11b,c,S4b,c–  
572 S9b,c), the deviation from the mean is not always in the same direction  
above and below  $D215$  or  $D175$ . Off Kollam, for example, the deviation of  
574 biomass at 40 m and 104 m is negative during February and August and  
positive during much of October in 2019; at other times, or over most of  
576 the year, the deviation has opposite signs (Fig. 11c). This tendency for the  
intraseasonal deviation to be of opposite sign at 40 m and 104 m is also seen  
578 often during the year at the other locations (Figs. S4c–S9c).

As expected, the variation of ZSS tends to be high when the variation  
580 of biomass above and below  $D215$  (or  $D175$ ) is in the same direction. An  
example is seen off Kollam in February 2019. The seasonal biomass devia-  
582 tion at both 40 m and 104 m is negative (Fig. 11a,c), leading to a negative  
deviation throughout February in the seasonal ZSS (Fig. 11f). The intrasea-  
584 sonal deviation is also largely negative during February, save a short-lived  
positive burst in the beginning of the second half of the month (Fig. 11b,c).  
586 As a result, the intraseasonal ZSS deviation is largely negative, but with a  
short-lived positive burst (Fig. 11f). The strong negative seasonal bias im-  
588 plies, however, a negative deviation in the daily ZSS throughout February  
2019 off Kollam (Fig. 11f). This possible cancellation of the deviation from  
590 the mean above and below  $D215$  (or  $D175$ ) leads to a weak variation in the  
intraseasonal SD [of ZSS](#) at the seven locations (Table S4); the SD is highest  
592 off Kollam and Jaigarh, but the ratio of the highest (Kollam) and lowest  
(Okha, Goa) intraseasonal SD is less than 1.4; in comparison, the ratio of  
594 the highest (Jaigarh) and lowest (Okha, Kanyakumari) seasonal SDs is over  
2.7 (Table S4).

596 Since the ZSS is an integral quantity, it is not surprising that its SD,  
whether seasonal or intraseasonal, is much smaller at  $\sim 5\%$  of the mean  
598 (Figs. 11f,S4f–S9f, Table S4). For comparison, the SD of biomass varies  
from  $\sim 15\text{--}20\%$  (Figs. 11c,S4c–S9c, Table S3).

## 600 6. Discussion

### 6.1. Summary

602 Though A22's data set covered a different period (2012–2020) than our  
data set (2017–2023), the monthly climatologies off Kollam, Goa, and Mum-

604 bai estimated using them are similar; the differences are relatively minor (see  
605 Section S1, Fig. S1). The additional four moorings provide a clearer picture  
606 of the south–north transition on the continental slope in the EAS; biomass  
607 is higher above  $D215$  or  $D175$ , which shallows during the summer monsoon  
608 in the SEAS and deepens during the winter monsoon in the NEAS, with the  
609 CEAS exhibiting a gradual transition between these two EAS regimes.

610 As noted by A22, the climatological ZSS is asymmetric in time, with  
611 the rise from the minimum during the summer monsoon occurring much  
612 faster than the gradual fall from the maximum during the winter monsoon  
613 (Fig. 5). This asymmetry, more pronounced in the NEAS and CEAS, leads  
614 to a strong intra-annual cycle, with peaks at around  $\sim 180$  days (the semi-  
615 annual cycle) and  $\sim 120$  days, in addition to the annual cycle (Figs. 6). The  
616 intra-annual band is stronger than the annual band within the seasonal cycle  
617 (Figs. 6,S2, Table S3).

618 The biomass also shows interannual variability off Kollam, Goa, and  
619 Mumbai, for which we have a record longer than a decade (2012–2023);  
620 these interannual variations affect the climatological averages. Year-to-year  
621 deviations from the monthly climatology are evident, with the most striking  
622 deviation occurring off Kollam in 2020, when the biomass was low over the  
623 entire deployment (see Section S3,[Fig. S10](#)). There is also variability at  
624 periods longer than the seasonal. The QBO reported off Kollam by A22  
625 is seen during 2012–2018; this QBO occurs sporadically off Mumbai and a  
626 weak signal is seen off Goa as well.

627 A key finding from the biomass data is the significant intraseasonal vari-  
628 ability (the 5–90-day band), which is at least comparable to the seasonal  
629 cycle (the 100–400-day band; Figs. 11,S4–S9, Table S3). The range of in-  
630 traseasonal variability is significantly higher off Kanyakumari owing to the

low seasonal range, but the intraseasonal and seasonal ranges are comparable off Kollam and Udupi in the SEAS. The intraseasonal range is higher than the seasonal range off Goa and Jaigarh in the CEAS, but they are again comparable in the NEAS (Table S3). This strong intraseasonal variability in biomass does not, however, lead to a comparably strong intraseasonal variability in the ZSS because the ZSS is determined by the variation both above and below  $D215$  (or  $D175$ ) and the deviation from mean is often in opposite directions (Figs. 11,S4–S9). The intraseasonal variability also includes sharp spikes for a day or more, but less than five days (Figs. 11e,S4e–S9e). Several of these spikes, which occur intermittently throughout the year, exceed one SD and some exceed even two SD.

#### 642    6.2. *The role of the physical forcing*

A22 showed that vertical movement of the climatological  $D215$  off Kollam, Goa, and Mumbai followed that of  $D23$ , the depth of the  $23^{\circ}\text{C}$  isotherm and therefore a measure of the vertical movement of the thermocline. This association also holds for our climatology of biomass (for  $D215$  or  $D175$ ) at all seven locations (Fig. 5). Our biomass climatology represents a different period than that of A22. Yet, this result still holds, implying that climatological upwelling and downwelling, which would move  $D23$  up and down, force a similar vertical movement of the climatological  $D215$  or  $D175$ , the contour separating the high-biomass upper ocean from the low-biomass lower ocean. Hence, in a climatological sense, we find validation for A22's result linking the physical forcing to the changes in biomass via the changes in oxygen as seen in the vertical movement of the oxycline (Fig. 5).

A proxy for  $D23$  is the sea level, which decreases (increases) or shows a negative (positive) anomaly during upwelling (downwelling), when  $D23$  rises

(falls) or moves up (down). As expected (see, for example, Shankar, 2000),  
658 the climatological SLA mirrors the climatological  $D_{23}$  (Fig. 5), suggesting  
the use of satellite-derived SLA as a proxy for  $D_{23}$ , for which a time series is  
660 not available on the continental slope of the EAS. A qualitative “eyeballing”  
of the data suggests that low (high) SLA, associated with upwelling (down-  
662 welling), co-occurs with high (low) biomass off Kollam in 2019 (Fig. 11d).  
To test this hypothesis, we carried out a wavelet coherence analysis to in-  
664 fer any possible link between the variation of SLA and biomass or ZSS at  
seasonal or intraseasonal time scales.

666 The analysis (figures not shown) did not show any conclusive relation.  
The coherence was weak and patchy even at the seasonal time scale. A  
668 possible reason for this lack of coherence is that the SLA, unlike biomass,  
is dominated by the annual cycle (the band picked by a **300-day low-pass**  
670 **300–400 days band-pass** filter) off Kollam, Goa, and Mumbai (Fig. 5). So it  
is not easy to quantify this expected relation between SLA and biomass at  
672 40 m even at the seasonal time scale.

Not surprisingly, this lack of coherence extends to intraseasonal vari-  
674 ability (Figs. 5,11d,S4d–S9d). Even during August–November 2018, when a  
seemingly “coherent” biomass variation seems to occur off Udupi, Goa, and  
676 Jaigarh in the intraseasonal band (Figs. 6,10; see Section 5.4), the coherence  
between SLA and biomass tends to be extremely patchy at these locations  
678 (figures not shown), making it difficult to draw unambiguous conclusions  
about the link between the vertical movement of the thermocline and the  
680 upper-ocean (above  $D_{215}$  or  $D_{175}$ ) biomass.

The above analysis, though inconclusive, leads to one useful conclusion:  
682 qualitative associations between variables may not imply a cause-and-effect  
relationship even if based on a sound theoretical basis.

684 *6.3. What sustains the zooplankton?*

Satellite-derived chlorophyll (chl-*a*) data are available as a daily time series, but with several gaps. Since these gaps preclude the creation of even a continuous, 10-day-low-pass time series, we use monthly chl-*a* data; daily data are plotted as curves where possible, but not subject to filtering or wavelet analysis. The lower temporal resolution implies that a significant part of the intraseasonal spectrum cannot be analysed.

Though one expects biomass and even ZSS to respond to chl-*a*, A22 showed that the relation is not straightforward. The long time series available off Kollam, Goa, and Mumbai shows that the biomass peaks do not necessarily follow the chl-*a* peaks (Fig. 9) even at the seasonal time scale resolved by the monthly time series. Neither is an increase in the magnitude of chl-*a* matched by an increase in that of the biomass at 40 m or of ZSS. Hence, wavelet coherence analysis (figures not shown) shows high wavelet coherence in the annual band, but the phase of chl-*a* does not lead that of biomass or ZSS, ruling out a quantitative cause-and-effect relationship. Yet, if we ignore this phase mismatch, there are instances when similar intraseasonal variation is seen in chl-*a* and biomass. Examples include high wavelet power at a period just above  $\sim$ 90 days off Kollam during the first half of 2019 and through most of 2021–2022. The classical food web is also active and sometimes dominant in determining the surface ocean biomass as seen in Kanyakumari during July 2019 (Fig. S4e,f). It is difficult, however, to see this relation unequivocally in these curves.

The biomass data at 40 m also show spikes — implying variability at periods shorter than five days (see Section 5.3) — throughout the year, irrespective of whether there is a seasonal or intraseasonal peak in chl-*a* (Figs. 11e,S4e–S9e). Examples include spikes exceeding two SD in the 40 m

biomass off Kollam towards the end of August and during September 2019,  
712 when the chl-*a* has already declined from its July seasonal peak (Fig. 11e).

Off Kanyakumari (Fig. S4c,d,), the biggest spike and the highest intraseasonal peak in the 40 m biomass occur during a short-lived increase in chl-*a*  
714 in September, but this chl-*a* peak is far weaker than the peak in July 2019,  
716 when the chl-*a* peak is over four times higher, but with smaller spikes and  
a weaker intraseasonal peak in the biomass at 40 m. A similar behaviour  
718 is seen at the other five locations (Figs. S5–S9): off Mumbai (Fig. S8), for  
example, the big spike in June 2019 precedes the increase in chl-*a* by several  
720 days.

One drawback of satellite chl-*a* data is that the satellite cannot see beyond  $\sim$ 30 m from the surface (maximum is  $\sim$ 40 m in clear water; André,  
722 1992), implying that not all of the phytoplankton biomass is part of the  
satellite estimate. Though the chl-*a* data set used here includes the pi-  
724 cophytoplankton, it cannot capture the picophytoplankton that dominate  
picophytoplankton, it cannot capture the picophytoplankton that dominate  
726 below  $\sim$ 40 m along with the microbial loop. Picoplankton (Campbell and  
Carpenter, 1986; Campbell et al., 1998; Bemal et al., 2018) and the micro-  
728 bial loop (Azam et al., 1983; Madhupratap et al., 1996a,b; Anil et al., 2021)  
have been shown to be important components of the marine food web in the  
730 Arabian Sea.

What the zooplankton biomass time series at these seven locations show  
732 is that the picophytoplankton and microbial loop must be dominating over  
the classical food web (Bemal et al., 2018; Anil et al., 2021) over a significant  
734 part of the year throughout the EAS. It is this non-classical part of the food  
web that probably sustains the significant intraseasonal bursts seen in the  
736 biomass data.

#### 6.4. Caveats and strengths

738 A22 discussed the caveats and strengths of using ADCP backscatter to map the variability of zooplankton biomass and standing stock.

740 They noted the lack of data in the near-surface regime, a consequence of the echoes from the air-sea interface. Since  $\sim 10\%$  of the range of the ADCP  
742 is lost, data are lost over the top  $\sim 20$  m for a 153.3 kHz ADCP moored at  
 $\sim 150$  m. Another limitation is that the cruises used for *in situ* sampling  
744 are restricted to one season, September–December, owing to the constraints imposed by weather conditions on mooring operations and availability of  
746 ship time. This limitation is partly obviated by the large range in backscatter and biomass over the sampled depth range from  $\sim 20$ –~~140~~24–~~140~~ m: the  
748 significant decrease in backscatter below  $D_{215}$  (or  $D_{175}$ ) leads to a range that is unlikely to be exceeded by sampling in other seasons. Yet, that  
750 zooplankton abundance and biomass are not necessarily related (see, for example, Madhupratap et al., 1990; Ambriz-Arreola et al., 2018) implies  
752 that the seasonal change in species can have an impact on the distribution of points in the scatter plot (Fig. 2). Analysis using ship-based sampling  
754 in the EAS (Jadhav and Smitha, 2024) shows a seasonal biomass difference of  $\sim 15$  mg m $^{-3}$ , comparable to our SD estimate of 14 mg m $^{-3}$  (Fig. 2).  
756 Therefore, it is unlikely that sampling in other seasons will lead to a major change in the backscatter-biomass regression, but it would be good to exploit  
758 any opportunity to broaden the sampling range. The absence of species information is, however, the most significant lacuna of the use of ADCP  
760 backscatter. Studies in the EAS show that even picoplankton are sufficiently differentiated that *Prochlorococcus* species attuned to low light do not bloom  
762 when exposed to high-nutrient conditions in the near-surface regime because of the light shock (Bemal et al., 2018). Even microbial communities show

764 similar sensitivity to environmental conditions (Khandeparker et al., 2025).

This biodiversity information is, nevertheless, lost even in satellite chl-*a* data, which are used to estimate the energy flux through the marine ecosystem. Zooplankton biomass estimated from acoustic backscatter provides the closest analogue to satellite chl-*a*. Thus, the chief merit of this method is obvious: traditional sampling cannot yield a time series of the kind presented above, precluding any analysis of the variability over the range of time scales seen in the backscatter data. For example, it is only with such a time series that it is possible to analyse the impact of climate modes like ENSO (El Niño Southern Oscillation; see, for example, Sikka, 1980) or the Indian-Ocean Dipole (IOD; Saji et al., 1999) on the interannual variation in zooplankton biomass and standing stock. In other words, the raw estimate of biomass is as biologically relevant — owing to its potential for estimating energy flux — as is the biodiversity that can be catalogued using MPN samples.

The time series of biomass, with its intraseasonal bursts and spikes, also calls into question the contours of biomass or ZSS drawn using cruise data. In the EAS, for example, it takes roughly a month to cover the Indian Exclusive Economic Zone (EEZ) from Kanyakumari to Okha (see, for example, Shetye et al., 1990, 1991; Vijith et al., 2022; Madhupratap et al., 1996a; Jyothibabu et al., 2010). It is certain, therefore, that this sampling cannot account for the spikes or the variability in at least the 5–30-day part of the intraseasonal band. This variability, evident at all mooring locations, implies that the error bar in these biomass or ZSS snapshots is likely too high to permit contouring of these variables using cruise data.

### 6.5. Epilogue

790        What we actually need is a synergy between the two methods because the  
791        two sets of information are not only complementary, but also relevant. This  
792        complementarity and relevance may be illustrated by the ADCP deployment  
793        off Kollam during October 2019 to December 2020. The backscatter —  
794        and therefore biomass — was low off Kollam throughout this deployment.  
795        Doubts regarding the instrument were generally laid to rest with a series of  
796        checks (see Section S3), but the clincher was the low biomass sampled using  
797        the MPN after deploying the ADCP in 2019 and before retrieving it in 2020  
798        (Table 2, Fig. 2). Indeed, it the time series that shows unambiguously that  
799        the biomass off Kollam was low throughout this 12–14-month period.

800        All methods — ship, satellite, or acoustics —, however, miss some in-  
801        formation. The obvious implication is that large parts of the marine food  
802        web, and therefore the energy flux through the marine ecosystem, is not  
803        measured. Some components, like picophytoplankton that are not captured  
804        in satellite chl-*a* and the microbial loop, are essentially unmeasurable. In  
805        this context, acoustic backscatter enables some constraints on the second  
806        trophic level, and our results from the EAS show that the picoplankton and  
807        microbial loop are critical for sustaining the observed zooplankton biomass  
808        and its variability. It is necessary for models to build the impact of even  
809        these difficult-to-measure or unmeasurable elements into their depiction of  
810        the marine food web in order to avoid the trap of the *McNamara fallacy*  
811        (Yankelovich, 1971).

**812 Declaration of competing interest**

The authors declare that they have no known competing financial interests or personal relationships that could have appeared to influence the work reported in this article.

**816 Acknowledgments**

This work was supported by ship time funded by CSIR (Council of Scientific and Industrial Research, New Delhi, India) and research funding from INCOIS (Indian National Centre for Ocean Information Services, Hyderabad, India) under the COSINE (Current Observations and Simulations in the Indian EEZ) project, which is a part of the OSMART programme of the Ministry of Earth Sciences. The ADCP moorings are maintained by our colleagues from the mooring group; they are assisted by the CSIR-NIO ship cell during cruises and the data are archived by Ashok Kankonkar. Rahul Khedekar assisted in processing the backscatter data and Roshan D'Souza in analysing the zooplankton samples. D. Shankar acknowledges the insights gained from conversations with Lidita Khandeparker on bacteria and the microbial loop and with A.C. Anil on marine ecosystems. Ranjan Kumar Sahu was supported by a fellowship from CSIR. This is CSIR-NIO contribution  
830 XXXX.

**References**

- 832 Almén, A.K., Tamelander, T., 2020. Temperature-related timing of the  
spring bloom and match between phytoplankton and zooplankton. Mar.  
834 Biol. Res. 16, 674–682. 10.1080/17451000.2020.1846201.

- Ambriz-Arreola, I., Gómez-Gutiérrez, J., Franco-Gordo, M., Plascencia-Palomera, V., Gasca, R., Kozak, E.R., Lavaniegos, B.E., 2018. Seasonal succession of tropical community structure, abundance, and biomass of five zooplankton taxa in the central Mexican Pacific. *Cont. Shelf Res.* 168, 54–67. [/10.1016/j.csr.2018.08.007](https://doi.org/10.1016/j.csr.2018.08.007).
- Amol, P., Bemal, S., Shankar, D., Jain, V., Thushara, V., Vijith, V., Vinayachandran, P.N., 2020. Modulation of chlorophyll concentration by down-welling Rossby waves during the winter monsoon in the southeastern Arabian Sea. *Prog. Oceanogr.* 186, 102365. [10.1016/j.pocean.2020.102365](https://doi.org/10.1016/j.pocean.2020.102365).
- Amol, P., Shankar, D., Fernando, V., Mukherjee, A., Aparna, S.G., Fernandes, R., Michael, G.S., Khalap, S.T., Satelkar, N.P., Agarvadekar, Y., Gaonkar, M.G., Tari, A.P., Kankonkar, A., Vernekar, S., 2014. Observed intraseasonal and seasonal variability of the West India Coastal Current on the continental slope. *J. Earth Syst. Sci.* 123, 1045–1074. [10.1007/s12040-014-0449-5](https://doi.org/10.1007/s12040-014-0449-5).
- André, J.M., 1992. Ocean color remote-sensing and the subsurface vertical structure of phytoplankton pigments. *Deep-Sea Res. Part A Oceanogr. Res. Pap.* 39, 763–779. [10.1016/0198-0149\(92\)90119-E](https://doi.org/10.1016/0198-0149(92)90119-E).
- Anil, A.C., Desai, D.V., Khandeparker, L., Krishnamurthy, V., Mapari, K., Mitbavkar, S., Patil, J.S., Sarma, V.V.S.S., Sawant, S.S., 2021. Short term response of plankton community to nutrient enrichment in central eastern Arabian Sea: Elucidation through mesocosm experiments. *J. Environ. Manage.* 288, 112390. [10.1016/j.jenvman.2021.112390](https://doi.org/10.1016/j.jenvman.2021.112390).
- Aparna, S.G., Desai, D.V., Shankar, D., Anil, A.C., Dora, S., Khedekar,

- 860 R.R., 2022. Seasonal cycle of zooplankton standing stock inferred from  
ADCP backscatter measurements in the eastern Arabian Sea. *Prog.*  
862 *Oceanogr.* 203, 102766. [10.1016/j.pocean.2022.102766](https://doi.org/10.1016/j.pocean.2022.102766).
- 864 Azam, F., Fenchel, T., Field, J.G., Gray, J.S., Meyer-Reil, L.A., Thingstad,  
F., 1983. The ecological role of water-column microbes in the sea. *Estuaries* 10, 257–263. [10.3384/meps010257](https://doi.org/10.3384/meps010257).
- 866 Banse, K., 1968. Hydrography of the Arabian Sea shelf of India and Pak-  
istan and effects on demersal fishes, in: Deep-Sea Res. *Oceanogr. Abstr.*,  
868 Elsevier. pp. 45–79. [10.1016/0011-7471\(68\)90028-4](https://doi.org/10.1016/0011-7471(68)90028-4).
- 870 Banse, K., 1995. Zooplankton: pivotal role in the control of ocean pro-  
duction: I. Biomass and production. *ICES J. Mar. Sci.* 52, 265–277.  
872 [10.1016/1054-3139\(95\)80043-3](https://doi.org/10.1016/1054-3139(95)80043-3).
- 874 Banse, K., English, D.C., 2000. Geographical differences in seasonality of  
CZCS-derived phytoplankton pigment in the Arabian Sea for 1978–1986.  
Deep-Sea Res. Part II Top. Stud. *Oceanogr.* 47, 1623–1677. [10.1016/S0967-0645\(99\)00157-5](https://doi.org/10.1016/S0967-0645(99)00157-5).
- 876 Banse, K., Postel, J.R., 2009. Wintertime convection and ventilation of the  
upper pycnocline in the northernmost Arabian Sea. *Geophysical Mono-*  
878 *graph Series* 185, 87–117. [10.1029/2008GM000704](https://doi.org/10.1029/2008GM000704).
- 880 Barber, R.T., Marra, J., Bidigare, R.C., Codispoti, L.A., Halpern, D., John-  
son, Z., Latasa, M., Goericke, R., Smith, S.L., 2001. Primary productivity  
and its regulation in the Arabian Sea during 1995. Deep-Sea Res. Part 2  
882 Top. Stud. *Oceanogr.* 48, 1127–1172. [10.1016/S0967-0645\(00\)00134-X](https://doi.org/10.1016/S0967-0645(00)00134-X).

- Batchelder, H.P., VanKeuren, J.R., Vaillancourt, R.D., Swift, E., 1995.
- 884      Spatial and temporal distributions of acoustically estimated zooplankton  
biomass near the marine light-mixed layers station ( $59^{\circ}30'N$ ,  $21^{\circ}00'W$ ) in  
886      the north Atlantic in May 1991. *J. Geophys. Res. Oceans* 100, 6549–6563.  
10.1029/94jc00981.
- 888      Bemal, S., Anil, A.C., Shankar, D., Remya, R., Roy, R., 2018. Picophytoplankton variability: Influence of winter convective mixing and advection in the northeastern Arabian Sea. *J. Mar. Syst.* 180, 37–48.  
890      10.1029/2001GL013422.
- 892      Bhalme, H.N., Rahalkar, S.S., Sikder, A.B., 1987. Tropical quasi-biennial oscillation of the 10-mb wind and Indian monsoon rainfall — implications  
894      for forecasting. *J. Climatol.* 7, 345–353. 10.1002/joc.3370070403.
- 896      Brock, J.C., McClain, C.R., 1992. Interannual variability in phytoplankton blooms observed in the northwestern Arabian Sea during the southwest monsoon. *J. Geophys. Res. Oceans* 97, 733–750. 10.1029/91JC02225.
- 898      Brock, J.C., McClain, C.R., Luther, M.E., Hay, W.W., 1991. The phytoplankton bloom in the northwestern Arabian Sea during the southwest monsoon of 1979. *J. Geophys. Res. Oceans* 96, 20623–20642.  
900      10.1029/91JC01711.
- 902      Campbell, L., Carpenter, E.J., 1986. Estimating the grazing pressure of heterotrophic nanoplankton on *Synechococcus* spp. using the sea water dilution and selective inhibitor techniques. *Mar. Ecol. Prog. Ser.* 33, 121–129.
- 906      Campbell, L., Landry, M.R., Constantinou, J., Nolla, H.A., Brown, S.L.,

- Liu, H., Caron, D.A., 1998. Response of microbial community structure  
908 to environmental forcing in the Arabian Sea. Deep-Sea Res. II Top. Stud.  
Oceanogr. 45, 2301–2325.
- 910 Chatterjee, A., Shankar, D., Shenoi, S.S.C., Reddy, G.V., Michael, G.S.,  
Ravichandran, M., Gopalkrishna, V.V., RamaRao, E.P., UdayaBhaskar,  
912 T.V.S., Sanjeevan, V.N., 2012. A new atlas of temperature and salinity  
for the North Indian Ocean. J. Earth Syst. Sci. 121, 559–593. 10.1007/  
914 s12040-012-0191-9.
- Chaudhuri, A., Shankar, D., Aparna, S.G., Amol, P., Fernando, V.,  
916 Kankonkar, A., Michael, G.S., Satelkar, N.P., Khalap, S.T., Tari, A.P.,  
Gaonkar, M.G., Ghatkar, S., Khedekar, R.R., 2020. Observed variability  
918 of the West India Coastal Current on the continental slope from 2009–  
2018. J. Earth Syst. Sci. 129, 57. 10.1007/s12040-019-1322-3.
- 920 Cisewski, B., Strass, V.H., Rhein, M., Krägesky, S., 2010. Seasonal variation  
of diel vertical migration of zooplankton from ADCP backscatter time  
922 series data in the Lazarev Sea, Antarctica. Deep-Sea Res. Part I Oceanogr.  
Res. Pap. 57, 78–94. 10.1016/j.dsr.2009.10.005.
- 924 Davis, R.E., Talley, L.D., Roemmich, D., Owens, W.B., Rudnick, D.L.,  
Toole, J., Weller, R., McPhaden, M.J., Barth, J.A., 2019. 100 years of  
926 progress in ocean observing systems. Meteorol. Monogr. 59, 3–1. 10.  
1175/AMSMONOGRAPH-D-18-0014.1.
- 928 Deines, K.L., 1999. Backscatter estimation using broadband acoustic  
Doppler current profilers, in: Proceedings of the IEEE Sixth Working  
930 Conference on Current Measurement (Cat. No. 99CH36331), IEEE. pp.  
249–253. 10.1109/CCM.1999.755249.

- 932 DeSousa, S.N., Dileepkumar, M., Sardessai, S., Sarma, V.V.S.S., Shirodkar,  
P.V., 1996. Seasonal variability in oxygen and nutrients in the central and  
934 eastern Arabian Sea. *Curr. Sci.* 71. [drs.nio.org/drs/handle/2264/35](http://drs.nio.org/drs/handle/2264/35).
- 936 Edvardsen, A., Slagstad, D., Tande, K.S., Jaccard, P., 2003. Assessing  
zooplankton advection in the Barents Sea using underway measurements  
and modelling. *Fish. Oceanogr.* 12, 61–74. [10.1046/j.1365-2419.2003.00219.x](https://doi.org/10.1046/j.1365-2419.2003.00219.x).
- 940 Flagg, C.N., Smith, S.L., 1989. On the use of the acoustic Doppler current  
profiler to measure zooplankton abundance. *Deep-Sea Res. Part A.*  
944 *Oceanogr. Res. Pap.* 36, 455–474. [10.1016/0198-0149\(89\)90047-2](https://doi.org/10.1016/0198-0149(89)90047-2).
- 942 García, H.E., Locarnini, R.A., Boyer, T.P., Antonov, J.I., Mishonov, A.V.,  
Baranova, O.K., Zweng, M.M., Reagan, J.R., Johnson, D.R., 2014. Dis-  
944 solved oxygen, apparent oxygen utilization, and oxygen saturation. NOAA  
Atlas NESDIS 75 3. [data.nodc.noaa.gov/woa/WOA18/DOC/woa18\\_vol3.pdf](http://data.nodc.noaa.gov/woa/WOA18/DOC/woa18_vol3.pdf).
- 946 Greene, C.H., Wiebe, P.H., Pelkie, C., Benfield, M.C., Popp, J.M.,  
948 1998. Three-dimensional acoustic visualization of zooplankton patch-  
iness. *Deep-Sea Res. Part II Top. Stud. Oceanogr.* 45, 1201–1217.  
950 [10.1016/S0967-0645\(98\)00034-4](https://doi.org/10.1016/S0967-0645(98)00034-4).
- 952 Greenlaw, C.F., 1979. Acoustical estimation of zooplankton populations 1.  
*Limnol. Oceanogr.* 24, 226–242. [10.4319/lo.1979.24.2.00226](https://doi.org/10.4319/lo.1979.24.2.00226).
- 954 Guerra, D., Schroeder, K., Borghini, M., Camatti, E., Pansera, M.,  
Schroeder, A., Sparnocchia, S., Chiggiato, J., 2019. Zooplankton diel  
vertical migration in the Corsica channel (north-western Mediterranean

- 956 Sea) detected by a moored acoustic Doppler current profiler. *Ocean Sci.*  
15, 631–649. [10.5194/os-15-631-2019](https://doi.org/10.5194/os-15-631-2019).
- 958 Hamilton, J.M., Collins, K., Prinsenberg, S.J., 2013. Links between ocean  
properties, ice cover, and plankton dynamics on interannual time scales  
960 in the Canadian Arctic Archipelago. *J. Geophys. Res. Oceans* 118, 5625–  
5639. [10.1002/jgrc.20382](https://doi.org/10.1002/jgrc.20382).
- 962 Hays, G.C., 2003. A review of the adaptive significance and ecosystem  
consequences of zooplankton diel vertical migrations, in: *Migrations and*  
964 *Dispersal of Marine Organisms: Proceedings of the 37th European Ma-*  
*rine Biology Symposium held in Reykjavík, Iceland, 5–9 August 2002,*  
966 *Springer.* pp. 163–170. [10.1007/978-94-017-2276-6\\_18](https://doi.org/10.1007/978-94-017-2276-6_18).
- 968 Heywood, K.J., Howe, S.S., Barton, E.D., 1991. Estimation of zooplankton  
abundance from shipborne ADCP backscatter. *Deep-Sea Res. Part A.*  
Oceanogr. Res. Pap. 38, 677–691. [10.1016/0198-0149\(91\)90006-2](https://doi.org/10.1016/0198-0149(91)90006-2).
- 970 Hobbs, L., Banas, N.S., Cohen, J.H., Cottier, F.R., Berge, J., Varpe, Ø.,  
2021. A marine zooplankton community vertically structured by light  
972 across diel to interannual timescales. *Biol. Lett.* 17, 20200810. [10.1098/rsbl.2020.0810](https://doi.org/10.1098/rsbl.2020.0810).
- 974 Hood, R.R., Beckley, L.E., Wiggert, J.D., 2017. Biogeochemical and ecolog-  
ical impacts of boundary currents in the Indian Ocean. *Prog. Oceanogr.*  
976 156, 290–325. [10.1016/j.pocean.2017.04.011](https://doi.org/10.1016/j.pocean.2017.04.011).
- 978 Inoue, R., Kitamura, M., Fujiki, T., 2016. Diel vertical migration of  
zooplankton at the S1 biogeochemical mooring revealed from acous-

- tic backscattering strength. *J. Geophys. Res. Oceans* 121, 1031–1050.  
980 10.1002/2015JC011352.
- Jadhav, S.J., Smitha, B., 2024. Abundance distribution pattern of zooplankton associated with the eastern Arabian Sea monsoon system as detected by underwater acoustics and net sampling. *Acoust. Aust.* , 1–  
982 2210.1007/s40857-024-00336-w.  
984
- Jiang, S., Dickey, T.D., Steinberg, D.K., Madin, L.P., 2007. Temporal variability of zooplankton biomass from ADCP backscatter time series data at the Bermuda Testbed Mooring site. *Deep-Sea Res. Part I Oceanogr. Res. Pap.* 54, 608–636. 10.1016/j.dsr.2006.12.011.  
986  
988
- Jyothibabu, R., Madhu, N.V., Habeebrehman, H., Jayalakshmy, K.V., Nair, K.K.C., Achuthankutty, C.T., 2010. Re-evaluation of ‘paradox of mesozooplankton’ in the eastern Arabian Sea based on ship and satellite observations. *J. Mar. Syst.* 81, 235–251. 10.1016/j.jmarsys.2009.12.019.  
990  
992
- Kang, M., Oh, S., Oh, W., Kang, D.J., Nam, S., Lee, K., 2024. Acoustic characterization of fish and macroplankton communities in the Seychelles-Chagos Thermocline Ridge of the southwest Indian Ocean. *Deep-Sea Res. Part II Top. Stud. Oceanogr.* 213, 105356. 10.1016/j.dsr2.2023.  
994  
996 105356.
- Keerthi, M.G., Lengaigne, M., Lévy, M., Vialard, J., Parvathi, V., de Boyer Montégut, C., Ethé, C., Aumont, O., Suresh, I., Akhil, V.P., Muraleedharan, P.M., 2017. Physical control of interannual variations of the winter chlorophyll bloom in the northern Arabian Sea. *Biogeosci.* 14, 3615–3632. 10.5194/bg-14-3615-2017.  
998  
1000  
1002

- Khandagale, P.A., Mhatre, V.D., Thomas, S., 2022. Seasonal and spatial  
1004 variability of zooplankton diversity in north eastern Arabian Sea along  
the Maharashtra coast. *J. Mar. Biol. Assoc. India* 64, 25–32. [mbai.org.in/php/journaldload.php?id=2618&bkid=128](http://mbai.org.in/php/journaldload.php?id=2618&bkid=128).
- Khandeparker, L., Kale, D., Hede, N., Anil, A.C., 2025. Application of functional metagenomics in the evaluation of microbial community dynamics  
1008 in the Arabian sea: Implications of environmental settings. *J. Environ. Manag.* 373, 123449. [10.1016/j.jenvman.2024.123449](https://doi.org/10.1016/j.jenvman.2024.123449).
- Kumar, S.P., Narvekar, J., 2005. Seasonal variability of the mixed layer  
1012 in the central Arabian Sea and its implication on nutrients and primary productivity. *Deep-Sea Res. Part II Top. Stud. Oceanogr.* 52, 1848–1861.  
1014 [10.1016/j.dsr2.2005.06.002](https://doi.org/10.1016/j.dsr2.2005.06.002). biogeochemical Processes in the Northern Indian Ocean.
- Lévy, M., Shankar, D., André, J.M., Shenoi, S.S.C., Durand, F.,  
1016 de Boyer Montégut, C., 2007. Basin-wide seasonal evolution of the  
1018 Indian Ocean's phytoplankton blooms. *J. Geophys. Res. Oceans* 112,  
[10.1029/2007JC004090](https://doi.org/10.1029/2007JC004090).
- Li, M., Gargett, A., Denman, K., 2000. What determines seasonal and  
1020 interannual variability of phytoplankton and zooplankton in strongly estuarine systems? *Estuar. Coast. Shelf Sci.* 50, 467–488. [10.1006/ecss.2000.0593](https://doi.org/10.1006/ecss.2000.0593).
- Liu, Y., Guo, J., Xue, Y., Sangmanee, C., Wang, H., Zhao, C., Khokiattiwong, S., Yu, W., 2022. Seasonal variation in diel vertical migration  
1024 of zooplankton and micronekton in the Andaman Sea observed by a

- moored ADCP. Deep-Sea Res. Part I Oceanogr. Res. Pap. 179, 103663.  
1028 10.1016/j.dsr.2021.103663.
- Madhupratap, M., Gopalakrishnan, T.C., Haridas, P., Nair, K.K.C., Ar-  
1030 avindakshan, P.N., Padmavati, G., Paul, S., 1996a. Lack of seasonal  
and geographic variation in mesozooplankton biomass in the Arabian  
1032 Sea and its structure in the mixed layer. Curr. Sci. 71, 863–868.  
[drs.nio.org/drs/handle/2264/2154](http://drs.nio.org/drs/handle/2264/2154).
- 1034 Madhupratap, M., Haridas, P., Ramaiah, N., Achuthankutty, C.T., 1992.  
Zooplankton of the southwest coast of India: abundance, composition,  
1036 temporal and spatial variability in 1987. Oceanogr. Indian Ocean .
- 1038 Madhupratap, M., Kumar, S.P., Bhattathiri, P.M.A., Kumar, M.D.,  
Raghukumar, S., Nair, K.K.C., Ramaiah, N., 1996b. Mechanism of the  
biological response to winter cooling in the northeastern Arabian Sea.  
1040 Nature 384, 549–552. 10.1038/384549a0.
- 1042 Madhupratap, M., Nair, S.R.S., Haridas, P., Padmavati, G., 1990. Response  
of zooplankton to physical changes in the environment: coastal upwelling  
along the central west coast of India. J. Coast. Res. , 413–426<http://www.jstor.org/stable/4297692>.
- 1044 Maraun, D., Kurths, J., 2004. Cross wavelet analysis: significance test-  
ing and pitfalls. Nonlin. Processes Geophys. 11, 505–514. 10.5194/  
npg-11-505-2004.
- 1046 McCreary, J.P., Kohler, K.E., Hood, R.R., Olson, D.B., 1996. A four-  
component ecosystem model of biological activity in the Arabian Sea.  
1050 Prog. Oceanogr. 37, 193–240. 10.1016/S0079-6611(96)00005-5.

- McCreary, J.P., Kundu, P.K., Molinari, R.L., 1993. A numerical investigation of dynamics, thermodynamics and mixed-layer processes in the Indian Ocean. *Prog. Oceanogr.* 31, 181–244. [10.1016/0079-6611\(93\)90002-U](https://doi.org/10.1016/0079-6611(93)90002-U).
- McCreary, J.P., Murtugudde, R., Vialard, J., Vinayachandran, P.N., Wiggert, J.D., Hood, R.R., Shankar, D., Shetye, S.R., 2009. Biophysical processes in the Indian Ocean. *Indian Ocean Biogeochem. Processes Ecol. Variab.* 185, 9–32. [10.1029/2008GM000768](https://doi.org/10.1029/2008GM000768).
- Mooley, D.A., Parthasarathy, B., 1984. Fluctuations in all-India summer monsoon rainfall during 1871–1978. *Clim. Change* 6, 287–301. [10.1007/BF00142477](https://doi.org/10.1007/BF00142477).
- Mukherjee, A., Shankar, D., Fernando, V., Amol, P., Aparna, S.G., Fernandes, R., Michael, G.S., Khalap, S.T., Satelkar, N.P., Agarvadekar, Y., Gaonkar, M.G., Tari, A.P., Kankonkar, A., Vernekar, S., 2014. Observed seasonal and intraseasonal variability of the East India Coastal Current on the continental slope. *J. Earth Syst. Sci.* 123, 1197–1232. [10.1007/s12040-014-0471-7](https://doi.org/10.1007/s12040-014-0471-7).
- Mukhopadhyay, S., Shankar, D., Aparna, S.G., Mukherjee, A., 2017. Observations of the sub-inertial, near-surface East India Coastal Current. *Cont. Shelf Res.* 148, 159–177. [10.1016/j.csr.2017.08.020](https://doi.org/10.1016/j.csr.2017.08.020).
- Mukhopadhyay, S., Shankar, D., Aparna, S.G., Mukherjee, A., Fernando, V., Kankonkar, A., Khalap, S., Satelkar, N.P., Gaonkar, M.G., Tari, A.P., Khedkar, R.R., Ghatkar, S., 2020. Observed variability of the East India Coastal Current on the continental slope during 2009–2018. *J. Earth Syst. Sci.* 129, 1–22. [10.1007/s12040-020-1346-8](https://doi.org/10.1007/s12040-020-1346-8).

- Nair, K.K.C., Madhupratap, M., Gopalakrishnan, T.C., Haridas, P., Gauns,  
1076 M., 1999. The Arabian Sea: physical environment, zooplankton and myc-  
trophid abundance. Indian J. Mar. Sci. 28, 138–145. [nopr.niscpr.res.  
in/handle/123456789/25690](http://nopr.niscpr.res.in/handle/123456789/25690).
- Nair, P.V., 1970. Primary productivity in the Indian seas. CMFRI Bulletin  
1080 22, 1–63. [eprints.cmfri.org.in/id/eprint/610](http://eprints.cmfri.org.in/id/eprint/610).
- Naqvi, S.W.A., Narvekar, P.V., Desa, E., 2006. Coastal biogeochemical pro-  
1082 cesses in the north Indian Ocean. Coastal segment (14°S–W), in: Robin-  
son, A.R., Brink, K.H. (Eds.), The Sea. John Wiley and Sons, Inc. vol-  
1084 ume 14. chapter 19, pp. 723–781.
- Naqvi, S.W.A., Noronha, R.J., Somasundar, K., Gupta, R.S., 1990. Sea-  
1086 sonal changes in the denitrification regime of the Arabian Sea. Deep-Sea  
Research 37, 593–611. [10.1016/0198-0149\(90\)90092-A](https://doi.org/10.1016/0198-0149(90)90092-A).
- Nie, L., Li, J., Wu, H., Zhang, W., Tian, Y., Liu, Y., Sun, P., Ye, Z., Ma, S.,  
1088 Gao, Q., 2023. The influence of ocean processes on fine-scale changes in  
the Yellow Sea cold water mass boundary area structure based on acoustic  
1090 observations. Rem. Sens. 15, 4272. [10.3390/rs15174272](https://doi.org/10.3390/rs15174272).
- Ohman, M.D., Hirche, H.J., 2001. Density-dependent mortality in an  
1092 oceanic copepod population. Nature 412, 638–641. [10.1038/35088068](https://doi.org/10.1038/35088068).
- Piontkovski, S.A., Williams, R., Melnik, T.A., 1995. Spatial heterogene-  
1094 ity, biomass and size structure of plankton of the Indian Ocean: some  
1096 general trends. Mar. Ecol. Prog. Ser. , 219–227 [www.jstor.org/stable/  
44634833](http://www.jstor.org/stable/44634833).

- 1098 Potiris, E., Frangoulis, C., Kalampokis, A., Ntoumas, M., Pettas, M., Peti-  
hakis, G., Zervakis, V., 2018. Acoustic doppler current profiler observa-  
1100 tions of migration patternsof zooplankton in the Cretan Sea. Ocean Sci.  
14, 783–800. [10.5194/os-14-783-2018](https://doi.org/10.5194/os-14-783-2018).
- 1102 Prasad, T., Bahulayan, N., 1996. Mixed layer depth and thermocline clima-  
tology of the Arabian Sea and western equatorial Indian Ocean. Indian J.  
1104 Mar. Sci. 25, 189–194. [nopr.niscpr.res.in/handle/123456789/37119](https://nopr.niscpr.res.in/handle/123456789/37119).
- 1106 Qasim, S.Z., 1977. Biological productivity of the Indian Ocean. Indian J.  
Mar. Sci. 6, 122–137. [nopr.niscpr.res.in/handle/123456789/39365](https://nopr.niscpr.res.in/handle/123456789/39365).
- 1108 Quéré, C.L., Andrew, R.M., Canadell, J.G., Sitch, S., Korsbakken, J.I.,  
Peters, G.P., Manning, A.C., Boden, T.A., Tans, P.P., Houghton, R.A.,  
2016. Global carbon budget 2016. Earth Syst. Sci. Data 8, 605–649.  
1110 [10.5194/essd-8-605-2016](https://doi.org/10.5194/essd-8-605-2016).
- 1112 Ramamurthy, S., 1965. Studies on the plankton of the North Kanara coast  
in relation to the pelagic fishery. J. Mar. Biol. Assoc. India 7, 127–149.  
[eprints.cmfri.org.in/id/eprint/894](https://eprints.cmfri.org.in/id/eprint/894).
- 1114 Rehim, M., Imran, M., 2012. Dynamical analysis of a delay model of  
phytoplankton-zooplankton interaction. Appl. Math. Model. 36, 638–647.  
1116 [10.1016/j.apm.2011.07.018](https://doi.org/10.1016/j.apm.2011.07.018).
- 1118 Rippeth, T.P., Simpson, J.H., 1998. Diurnal signals in vertical motions  
on the Hebridean shelf. Limnol. Oceanogr. 43, 1690–1696. [10.4319/lo.1998.43.7.1690](https://doi.org/10.4319/lo.1998.43.7.1690).
- 1120 Rochford, D., 1964. Salinity maxima in the upper 1000 metres of the north

- Indian Ocean. Marine and Freshwater Research 15, 1–24. 10.1071/  
1122 MF9640001.
- Ryther, J.H., Hall, J.R., Pease, A.K., Bakun, A., Jones, M.M., 1966.  
1124 Primary organic production in relation to the chemistry and hydrogra-  
phy of the western Indian Ocean. Limnol. and Oceanogr. 11, 371–380.
- 1126 10.4319/lo.1966.11.3.0371.
- Saji, N.H., Goswami, B.N., Vinayachandran, P.N., Yamagata, T., 1999. A  
1128 dipole mode in the tropical Indian Ocean. Nature 401, 360–363. 10.1038/  
43854.
- 1130 Schmidt, H., Czeschel, R., Visbeck, M., 2020. Seasonal variability of the  
Arabian Sea intermediate circulation and its impact on seasonal changes  
1132 of the upper oxygen minimum zone. Ocean Sci. 16, 1459–1474. 10.5194/  
os-16-1459-2020.
- 1134 Shankar, D., 2000. Seasonal cycle of sea level and currents along the coast  
of India. Current Science 78, 279–288.
- 1136 Shankar, D., Remya, R., Anil, A.C., Vijith, V., 2019. Role of physical  
processes in determining the nature of fisheries in the eastern Arabian  
1138 Sea. Prog. Oceanogr. 172, 124–158. 10.1016/j.pocean.2018.11.006.
- Shankar, D., Remya, R., Vinayachandran, P.N., Chatterjee, A., Behera, A.,  
1140 2016. Inhibition of mixed-layer deepening during winter in the north-  
eastern Arabian Sea by the West India Coastal Current. Clim. Dyn. 47,  
1142 1049–1072. 10.1007/s00382-015-2888-3.
- Shankar, D., Shenoi, S.S.C., Nayak, R.K., Vinayachandran, P.N., Nam-  
1144 poothiri, G., Almeida, A.M., Michael, G.S., Kumar, M.R.R., Sun-

- dar, D., Sreejith, O.P., 2005. Hydrography of the eastern Arabian  
1146 Sea during summer monsoon 2002. J. Earth Syst. Sci. 114, 459–474.  
10.1007/BF02702023.
- 1148 Shankar, D., Shetye, S.R., 1997. On the dynamics of the Lakshadweep high  
and low in the southeastern Arabian Sea. J. Geophys. Res. Oceans 102,  
1150 12551–12562. 10.1029/97JC00465.
- 1152 Shankar, D., Vinayachandran, P., Unnikrishnan, A., 2002. The monsoon  
currents in the north Indian Ocean. Prog. in ocean. 52, 63–120. 10.1016/  
1154 S0079-6611(02)00024-1.
- 1156 Shenoi, S.S.C., Shankar, D., Michael, G.S., Kurian, J., Varma, K.K., Kumar,  
M.R.R., Almeida, A.M., Unnikrishnan, A.S., Fernandes, W., Barreto, N.,  
Gnanaseelan, C., Mathew, R., Praju, K.V., Mahale, V., 2005. Hydrogra-  
phy and water masses in the southeastern Arabian Sea during March–June  
1158 2003. J. Earth Syst. Sci. 114, 475–491. 10.1007/BF02702024.
- 1160 Shenoi, S.S.C., Shankar, D., Shetye, S.R., 2004. Remote forcing annihilates  
barrier layer in southeastern Arabian Sea. Geophys. Res. Lett. 10.1029/  
2003GL019270.
- 1162 Shetye, S.R., Gouveia, A.D., Shenoi, S.S.C., 1992. Does winter cool-  
ing lead to the subsurface salinity minimum off Saurashtra, India?  
1164 Oceanogr. Indian Ocean , 617–625drs.nio.org/drs/bitstream/2264/  
3139/2/Oceanogr\_Indian\_Ocean\_1992\_617.pdf.
- 1166 Shetye, S.R., Gouveia, A.D., Shenoi, S.S.C., Michael, G.S., Sundar, D.,  
Almeida, A.M., Santanam, K., 1991. The coastal current off western

- 1168 India during the northeast monsoon. Deep-Sea Res. Part A. Oceanogr.  
Res. Pap. 38, 1517–1529. [10.1016/0198-0149\(91\)90087-V](https://doi.org/10.1016/0198-0149(91)90087-V).
- 1170 Shetye, S.R., Gouveia, A.D., Shenoi, S.S.C., Sundar, D., Michael, G.S.,  
Almeida, A., Santanam, K., 1990. Hydrography and circulation off the  
1172 west coast of India during the southwest monsoon 1987. J. Mar. Res. 48,  
359–378.
- 1174 Shi, W., Wang, M., 2022. Phytoplankton biomass dynamics in the Arabian  
Sea from VIIRS observations. J. Mar. Syst. 227, 103670. [10.1016/j.jmarsys.2021.103670](https://doi.org/10.1016/j.jmarsys.2021.103670).
- 1176 Sikka, D.R., 1980. Some aspects of the large scale fluctuations of sum-  
1178 mer monsoon rainfall over India in relation to fluctuations in the plan-  
etary and regional scale circulation parameters. Proceedings of the In-  
1180 dian Academy of Sciences (Earth and Planetary Sciences) 89, 179–195.  
[10.1007/BF02913749](https://doi.org/10.1007/BF02913749).
- 1182 Smeti, H., Pagano, M., Menkes, C., Dhaussy, A.L., Hunt, B.P.V., Allain, V.,  
Rodier, M., De Boissieu, F., Kestenare, E., Sammari, C., 2015. Spatial  
1184 and temporal variability of zooplankton off New Caledonia (Southwestern  
Pacific) from acoustics and net measurements. J. Geophys. Res. Oceans  
1186 120, 2676–2700. [10.1002/2014JC010441](https://doi.org/10.1002/2014JC010441).
- Smith, S.L., Madhupratap, M., 2005. Mesozooplankton of the Arabian  
1188 Sea: patterns influenced by seasons, upwelling, and oxygen concentra-  
tions. Prog. Oceanogr. 65, 214–239. [10.1016/j.pocean.2005.03.007](https://doi.org/10.1016/j.pocean.2005.03.007).
- 1190 Sreenivas, P., Patnaik, K.V.K.R.K., Prasad, K.V.S.R., 2008. Monthly vari-

- ability of mixed layer over Arabian Sea using ARGO data. Mar. Geod.  
1192 31, 17–38. 10.1080/01490410701812311.
- Subrahmanyam, R., 1959. Studies on the phytoplankton of the west coast of  
1194 India: Part II. Physical and chemical factors influencing the production  
of phytoplankton, with remarks on the cycle of nutrients and on the re-  
1196 lationship of the phosphate-content to fish landings, in: Proc. Ind. Acad.  
Sci., Springer. pp. 189–252. 10.1007/BF03051925.
- 1198 Subrahmanyam, R., Sarma, A.H., 1960. Studies on the phytoplankton of the  
west coast of India. Part III. Seasonal variation of the phytoplankters and  
1200 environmental factors. Indian J. Fish. 7, 307–336. [eprints.cmfri.org.in/1899/](http://eprints.cmfri.org.in/1899/).
- 1202 Torrence, C., Compo, G.P., 1998. A practical guide to wavelet analysis. Bull.  
Am. Meteorol. Soc. 79, 61–78. 10.1175/1520-0477(1998)079<0061:  
1204 APGTWA>2.0.CO;2.
- 1206 Ursella, L., Cardin, V., Batistić, M., Garić, R., Gačić, M., 2018. Evidence of  
zooplankton vertical migration from continuous Southern Adriatic buoy  
current-meter records. Prog. Oceanogr. 167, 78–96. 10.1016/j.pocean.  
1208 2018.07.004.
- 1210 Ursella, L., Pensieri, S., Pallàs-Sanz, E., Herzka, S.Z., Bozzano, R., Tenreiro,  
M., Cardin, V., Candela, J., Sheinbaum, J., 2021. Diel, lunar and seasonal  
vertical migration in the deep western Gulf of Mexico evidenced from  
1212 a long-term data series of acoustic backscatter. Prog. Oceanogr. 195,  
102562. 10.1016/j.pocean.2021.102562.
- 1214 Vijith, V., Shetye, S.R., Gouveia, A.D., Shenoi, S.S.C., Michael, G.S., Sun-

- dar, D., 2022. Circulation in the region of the West India Coastal Current  
1216 in March 1994 hydrographic and altimeter data. *J. Earth Syst. Sci.* 131,  
16. [10.1007/s12040-021-01761-5](https://doi.org/10.1007/s12040-021-01761-5).
- 1218 Vijith, V., Vinayachandran, P.N., Thushara, V., Amol, P., Shankar, D.,  
Anil, A.C., 2016. Consequences of inhibition of mixed-layer deepening  
1220 by the West India Coastal Current for winter phytoplankton bloom in  
the northeastern Arabian Sea. *J. Geophys. Res. Oceans* 121, 6583–6603.  
1222 [10.1002/2016JC012004](https://doi.org/10.1002/2016JC012004).
- 1224 Wiebe, P.H., Greene, C.H., Stanton, T.K., Burczynski, J., 1990. Sound  
scattering by live zooplankton and micronekton: empirical studies with  
a dual-beam acoustical system. *The Journal of the Acoustical Society of  
1226 America* 88, 2346–2360. [10.1121/1.400077](https://doi.org/10.1121/1.400077).
- 1228 Winder, M., Schindler, D.E., 2004. Climatic effects on the phenology of lake  
processes. *Global Change Biol.* 10, 1844–1856. [10.1111/j.1365-2486.2004.00849.x](https://doi.org/10.1111/j.1365-2486.2004.00849.x).
- 1230 Wishner, K.F., Gowing, M.M., Gelfman, C., 1998. Mesozooplankton  
biomass in the upper 1000 m in the Arabian Sea: overall seasonal and  
1232 geographic patterns, and relationship to oxygen gradients. *Deep-Sea Res.  
Part II Top. Stud. Oceanogr.* 45, 2405–2432. [10.1016/S0967-0645\(98\)  
1234 00078-2](https://doi.org/10.1016/S0967-0645(98)00078-2).
- 1236 Wyrtki, K., Bennett, E.B., Rochford, D.J., Expedition, I.I.O., (U.S.),  
N.S.F., of Hawaii (Honolulu), U., 1971. Oceanographic atlas of the  
International Indian Ocean Expedition. National Science Foundation.  
1238 [//cir.nii.ac.jp/crid/1130000796355741312](https://cir.nii.ac.jp/crid/1130000796355741312).

Yankelovich, D., 1971. Interpreting the New Life Styles. Sales Management,  
1240 the Marketing Magazine, Dartnell Corporation. [https://en.wikipedia.org/wiki/McNamara\\_fallacy](https://en.wikipedia.org/wiki/McNamara_fallacy).

**Table 1:** ADCP deployment details at the respective locations are shown in this table. All ADCPs operated at 153.3 kHz with a 1 hour interval, and vertical bin size of 4 m. Moorings were deployed on the continental slope at depths of approximately 950–1200 m and serviced annually, subject to ship availability. The sixth column lists the reference echo intensity (Er) for each beam, and the seventh column provides the corresponding RSSI conversion factor (Deines, 1999).

Station (Position; °E, °N)	Date		Depth (in m)			Kc
	Deployment	Recovery	Ocean	ADCP	Er	
Okha (67.47, 22.26)	01/10/2018	01/12/2019	996	118	37 , 37 , 37 , 36	0.42 , 0.44 , 0.42 , 0.43
	01/12/2019	04/12/2020	1166	312	39 , 36 , 38 , 36	0.42 , 0.44 , 0.42 , 0.43
	04/12/2020	08/03/2022	1021	144	41 , 37 , 38 , 37	0.42 , 0.44 , 0.42 , 0.43
	08/03/2022	01/01/2023	1019	142	37 , 38 , 39 , 36	0.42 , 0.44 , 0.42 , 0.43
	01/01/2023	11/12/2023	1072	200	37 , 40 , 42 , 37	0.42 , 0.44 , 0.42 , 0.43
Mumbai (69.24, 20.01)	09/11/2017	29/09/2018	1025	150	36 , 34 , 39 , 42	0.40 , 0.40 , 0.40 , 0.40
	29/09/2018	29/11/2019	1122	125	35 , 36 , 39 , 42	0.40 , 0.40 , 0.40 , 0.40
	29/11/2019	02/12/2020	1143	164	37 , 34 , 39 , 43	0.40 , 0.40 , 0.40 , 0.40
	02/12/2020	06/03/2022	1125	142	36 , 34 , 39 , 42	0.40 , 0.40 , 0.40 , 0.40
	07/03/2022	02/01/2023	1103	158	37 , 34 , 40 , 43	0.40 , 0.40 , 0.40 , 0.40
	02/01/2023	09/12/2023	1091	944	35 , 37 , 40 , 43	0.40 , 0.40 , 0.40 , 0.40
Jaigarh (71.12, 17.53)	27/10/2017	27/09/2018	1039	198	32 , 35 , 33 , 32	0.45 , 0.45 , 0.45 , 0.45
	27/09/2018	30/10/2019	1032	164	32 , 35 , 33 , 31	0.45 , 0.45 , 0.45 , 0.45
	03/11/2019	30/11/2020	1142	264	32 , 36 , 33 , 32	0.45 , 0.45 , 0.45 , 0.45
	30/11/2020	05/03/2022	1099	119	33 , 36 , 34 , 32	0.45 , 0.45 , 0.45 , 0.45
Goa (72.74, 15.17)	03/10/2017	25/09/2018	1000	174	35 , 37 , 34 , 35	0.44 , 0.44 , 0.40 , 0.41
	25/09/2018	16/10/2019	969	145	38 , 36 , 36 , 34	0.44 , 0.44 , 0.40 , 0.41
	16/10/2019	29/11/2020	966	143	44 , 38 , 36 , 43	0.44 , 0.44 , 0.40 , 0.41
	29/11/2020	03/03/2022	985	157	35 , 40 , 35 , 38	0.44 , 0.44 , 0.40 , 0.41
	03/03/2022	05/01/2023	984	159	35 , 38 , 35 , 34	0.44 , 0.44 , 0.40 , 0.41
	05/01/2023	14/12/2023	996	195	36 , 38 , 36 , 35	0.44 , 0.44 , 0.4 , 0.41
Udupi (74.04, 12.5)	05/10/2017	06/10/2018	1028	176	44 , 46 , 29 , 35	0.45 , 0.45 , 0.45 , 0.45
	06/10/2018	18/10/2019	1027	179	32 , 38 , 30 , 36	0.45 , 0.45 , 0.45 , 0.45
	18/10/2019	11/12/2020	1018	168	33 , 37 , 31 , 38	0.45 , 0.45 , 0.45 , 0.45
	11/03/2022	06/01/2023	1036	155	31 , 32 , 32 , 33	0.45 , 0.45 , 0.45 , 0.45
	06/01/2023	15/12/2023	1035	882	31 , 33 , 32 , 34	0.45 , 0.45 , 0.45 , 0.45
Kollam (75.44, 9.05)	07/10/2017	08/10/2018	1174	200	43 , 55 , 45 , 43	0.49 , 0.50 , 0.49 , 0.50
	08/10/2018	20/10/2019	1160	123	49 , 62 , 46 , 46	0.49 , 0.50 , 0.49 , 0.50
	20/10/2019	13/12/2020	1209	176	52 , 61 , 54 , 55	0.49 , 0.50 , 0.49 , 0.50
	13/12/2020	13/03/2022	1129	91	49 , 51 , 46 , 47	0.49 , 0.50 , 0.49 , 0.50
	13/03/2022	08/01/2023	1149	164	41 , 48 , 43 , 41	0.49 , 0.50 , 0.49 , 0.50
	08/01/2023	17/12/2023	1171	987	41 , 45 , 43 , 41	0.49 , 0.50 , 0.49 , 0.50
Kanyakumari (77.39, 6.96)	08/10/2017	10/10/2018	1055	181	32 , 34 , 38 , 35	0.45 , 0.45 , 0.45 , 0.45
	10/10/2018	22/10/2019	1075	180	36 , 34 , 39 , 36	0.45 , 0.45 , 0.45 , 0.45
	22/10/2019	14/12/2020	1060	167	33 , 35 , 36 , 35	0.45 , 0.45 , 0.45 , 0.45
	14/12/2020	14/03/2022	1184	287	34 , 36 , 36 , 35	0.45 , 0.45 , 0.45 , 0.45

**Table 2:** Volumetric zooplankton samples collected from various stations. Sampling depths were standardized in later years to the following **binsdepth ranges**: 0–25 m, 25–50 m, 50–75 m, 75–100 m, and 100–150 m. Abbreviations: Okha (O), Mumbai (M), Jaigarh (J), Goa (G), Udupi (U), Kollam (K), Kanyakumari (KK); numeric tags denote specific station cruises.

Sample number	Tag	Lat ( $^{\circ}$ N)	Lon ( $^{\circ}$ E)	Date	Time (IST)	Sampling depth range (m)
1-3	G1	15.18	72.79	25 Sep 18	0452	50 – 25, 100 – 50, 150 – 100
4-6	G2	15.16	72.71	25 Sep 18	2108	50 – 25, 100 – 50, 150 – 100
7-10	G2	15.16	72.71	25 Sep 18	2137	40 – 20, 60 – 40, 80 – 60, 100 – 80
11-14	J1	—	—	26 Sep 18	2000	40 – 20, 60 – 40, 80 – 60, 100 – 80
15-17	J2	—	—	27 Sep 18	2000	50 – 25, 100 – 50, 150 – 100
18-21	J2	—	—	27 Sep 18	2100	40 – 20, 60 – 40, 80 – 60, 100 – 80
22-25	M1	20.00	69.19	28 Sep 18	2135	40 – 20, 60 – 40, 80 – 60, 100 – 80
26-27	M1	20.00	69.19	28 Sep 18	2205	50 – 25, 100 – 50
28-29	M2	20.01	69.20	29 Sep 18	2035	50 – 25, 100 – 50
30-33	M2	20.01	69.20	29 Sep 18	2057	40 – 20, 60 – 40, 80 – 60, 100 – 80
34-37	U1	—	—	5 Oct 18	2000	40 – 20, 60 – 40, 80 – 60, 100 – 80
38-40	U1	—	—	5 Oct 18	2100	50 – 25, 100 – 50, 150 – 100
41-43	U2	—	—	6 Oct 18	2000	50 – 25, 100 – 50, 150 – 100
44-47	U2	—	—	6 Oct 18	2100	40 – 20, 60 – 40, 80 – 60, 100 – 80
48-51	K1	9.06	75.42	8 Oct 18	0421	40 – 20, 60 – 40, 80 – 60, 100 – 80
52-54	K1	9.06	75.42	8 Oct 18	0449	50 – 25, 100 – 50, 150 – 100
55-56	K2	9.04	75.40	8 Oct 18	2027	50 – 25, 100 – 50
57-60	K2	9.04	75.40	8 Oct 18	2045	40 – 20, 60 – 40, 80 – 60, 100 – 80
61-64	G2	15.16	72.74	16 Oct 19	0829	50 – 25, 75 – 50, 100 – 75, 150 – 100
65-67	G3	15.16	72.74	16 Oct 19	1812	50 – 25, 75 – 50, 100 – 75
68-70	K2	9.02	75.42	20 Oct 19	0840	50 – 25, 75 – 50, 100 – 75
71-74	K3	9.04	75.43	20 Oct 19	1934	50 – 25, 75 – 50, 100 – 75, 150 – 100
75-78	KK1	—	—	22 Oct 19	0742	50 – 25, 75 – 50, 100 – 75, 150 – 100
79-82	KK2	—	—	22 Oct 19	1925	50 – 25, 75 – 50, 100 – 75, 150 – 100
83-86	J1	—	—	30 Oct 19	0324	50 – 25, 75 – 50, 100 – 75, 150 – 100
87-89	J2	—	—	4 Nov 19	0946	75 – 50, 100 – 75, 150 – 100
90-92	M2	19.98	69.22	29 Nov 19	1434	50 – 25, 75 – 50, 100 – 75
93-96	M3	20.01	69.23	30 Nov 19	0958	50 – 25, 75 – 50, 100 – 75, 150 – 100
97-100	O1	22.24	67.49	1 Dec 19	0937	50 – 25, 75 – 50, 100 – 75, 150 – 100
101	O2	22.25	67.46	1 Dec 19	1957	150 – 100
102-105	G3	15.68	73.22	28 Nov 20	0930	50 – 25, 75 – 50, 100 – 75, 150 – 100
105-108	G4	15.32	73.22	29 Nov 20	1558	50 – 25, 75 – 50, 100 – 75, 150 – 100
108-110	J2	17.85	71.21	30 Nov 20	1458	75 – 50, 100 – 75, 150 – 100
111-114	J3	17.91	71.21	1 Dec 20	1052	50 – 25, 75 – 50, 100 – 75, 150 – 100
115-118	M4	20.03	69.38	2 Dec 20	2016	50 – 25, 75 – 50, 100 – 75, 150 – 100
119	O2	22.41	67.80	4 Dec 20	0953	150 – 100
120-123	O3	22.41	67.79	4 Dec 20	2011	50 – 25, 75 – 50, 100 – 75, 150 – 100
124-127	K3	9.11	75.72	12 Dec 20	2335	50 – 25, 75 – 50, 100 – 75, 150 – 100
128-131	K4	9.06	75.74	13 Dec 20	1507	50 – 25, 75 – 50, 100 – 75, 150 – 100
132-134	KK1	7.62	77.63	14 Dec 20	1226	50 – 25, 75 – 50
135-138	KK2	7.62	77.63	14 Dec 20	2047	50 – 25, 75 – 50, 100 – 75, 150 – 100
139-142	G4	15.32	73.21	3 Mar 22	0823	50 – 25, 75 – 50, 100 – 75, 150 – 100
143-146	G5	15.68	73.21	4 Mar 22	1030	50 – 25, 75 – 50, 100 – 75, 150 – 100
147-150	M5	19.99	69.23	7 Mar 22	0957	50 – 25, 75 – 50, 100 – 75, 150 – 100
151-154	O3	22.24	67.50	8 Mar 22	0806	50 – 25, 75 – 50, 100 – 75, 150 – 100
155-158	U3	12.50	74.04	12 Mar 22	1156	50 – 25, 75 – 50, 100 – 75, 150 – 100

159-160	K4	9.04	75.42	13 Mar 22	1027	$50 - 25, 75 - 50, 100 - 75$
165-168	G7	–	–	5 Jan 23	1935	$50 - 25, 75 - 50, 100 - 75, 150 - 100$
169-172	J4	–	–	4 Jan 23	1134	$50 - 25, 75 - 50, 100 - 75, 150 - 100$
173-176	M6	–	–	2 Jan 23	1950	$50 - 25, 75 - 50, 100 - 75, 150 - 100$
177-180	U4	–	–	6 Jan 23	1538	$50 - 25, 75 - 50, 100 - 75, 150 - 100$
181-184	K5	–	–	8 Jan 23	1156	$50 - 25, 75 - 50, 100 - 75, 150 - 100$

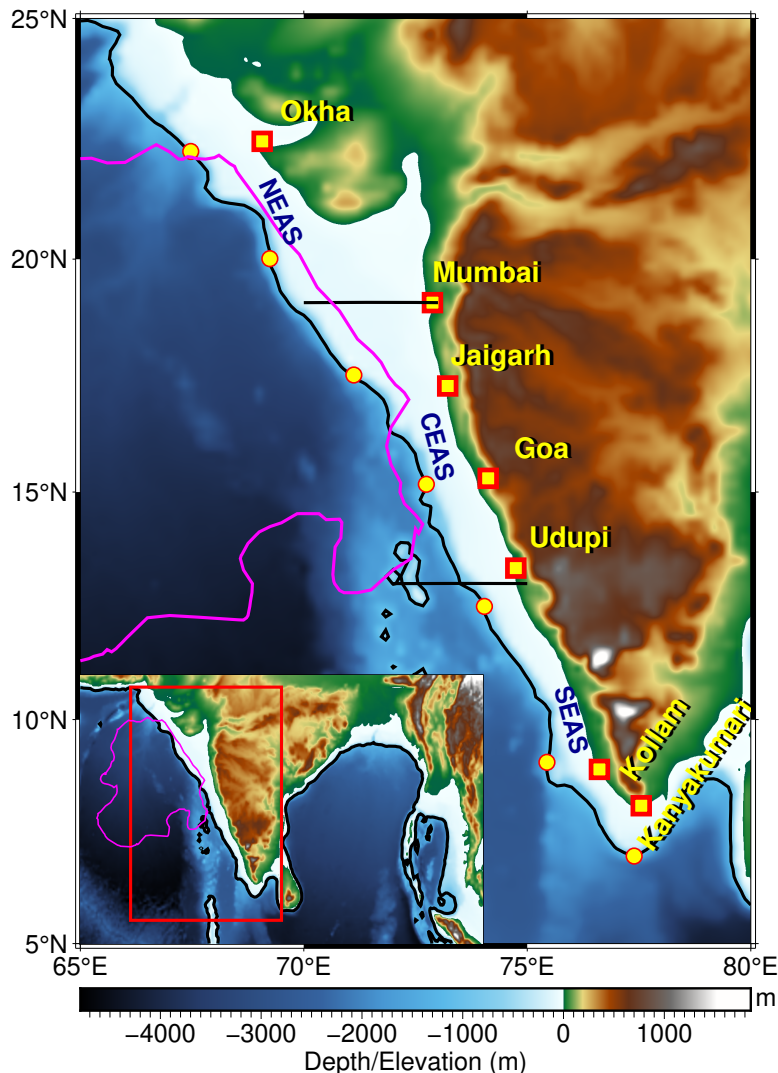


**Figure 1:** Map showing The map illustrates the study region of interest in the eastern Arabian Sea. Slope (EAS), where slope moorings are deployed at positioned along the ~1000 m depth isobath, indicated as shown by black bathymetry contours. Shelf width increases poleward. The continental shelf widens progressively toward the north along the Indian west coast. Mooring sites locations off Okha and Mumbai are situated in the northeastern Arabian Sea (NEAS), those off Jaigarh and Goa in the central Arabian Sea (CEAS), and those off Kollam and Kanyakumari in the southeastern Arabian Sea (SEAS). Udupi lies just north of transition line between the boundary separating the CEAS and SEAS. The oxygen minimum zone (OMZ) is marked outlined by the area enclosed within magenta contours, following A22 (Naqvi et al., 1990; Smith and Madhupratap, 2005).

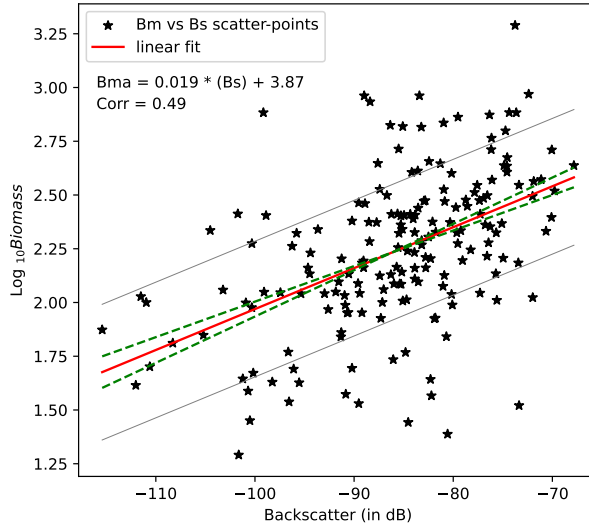


**Figure 2:** A linear regression of biomass ( $\log_{10}$  scale) and backscattering acoustic backscatter strength (in dB) is shown. The fit lies within the error uncertainty bounds of Aparna et al. (2022) reported by A22, who used 67 data points; the updated analysis uses an expanded dataset of 184 points with newly appended incorporating additional volumetric zooplankton samples.  $Bs$  is ADCP backscatter, and  $Bma$  zooplankton biomass derived from the former. The regression best-fit equation is  $y = 0.019x + 3.87$ , with a correlation coefficient of 0.49. The  $\pm 1$  SD of linear regressed line shown in parallel grey lines. Dashed green lines indicate the error bounds of denote the uncertainty in slope and intercept. This range leads to estimates corresponding to an estimated approximate biomass uncertainty of  $\sim 14 \text{ mg m}^{-3}$  in biomass. The standard deviation of SD in  $\log_{10}(\text{Biomass})$  is  $\pm 0.49$ , corresponding translating to a backscatter range of 48.58 dB, encompassing. This range spans the full extent of observed range and backscatter values, supporting the robustness reliability of biomass dependence on using ADCP-derived backscatter as a proxy for zooplankton biomass.

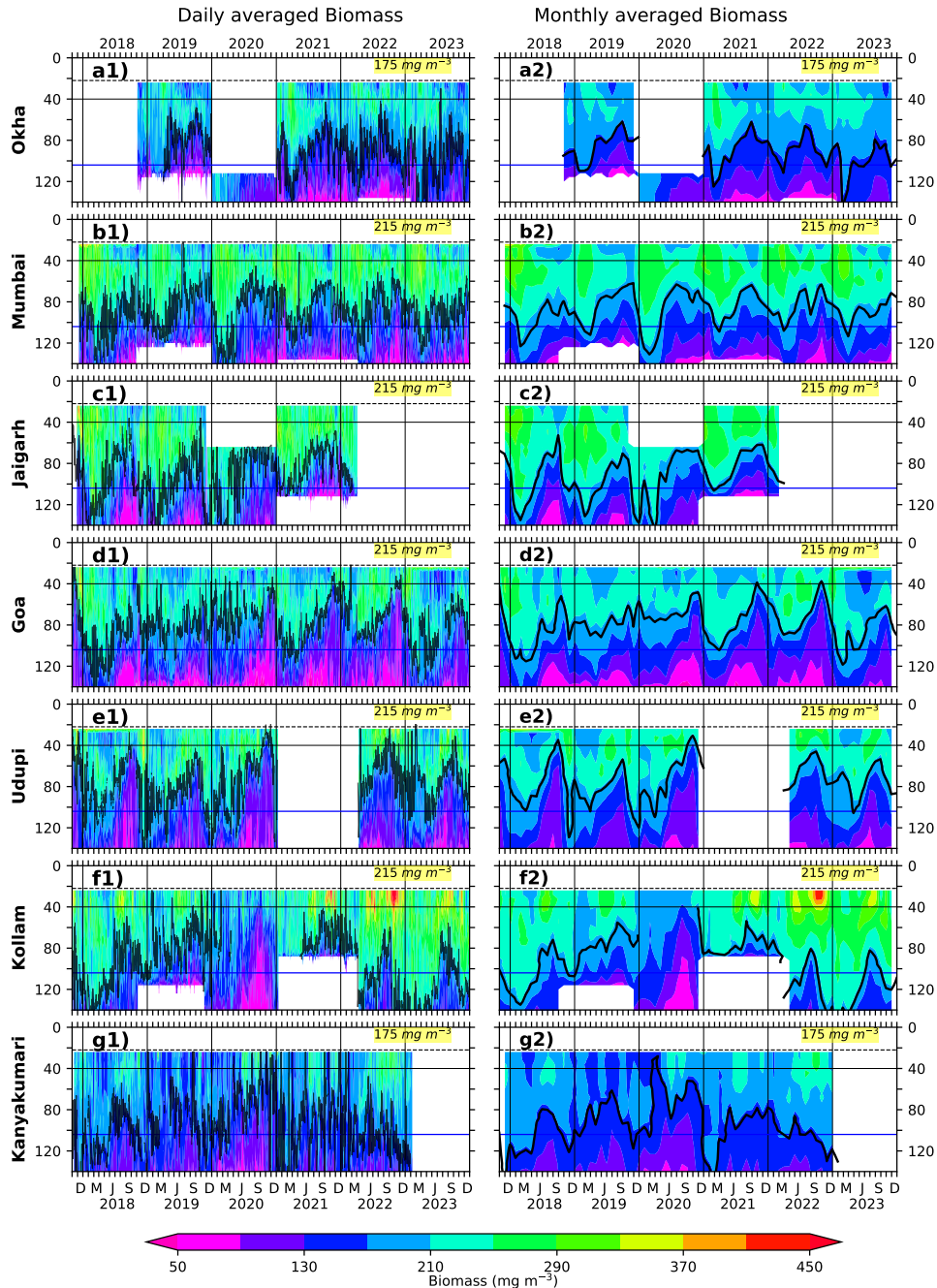


**Figure 3:** Daily and monthly averaged biomass for at the EAS moorings arranged by mooring sites, from north (top) to south (bottom), are presented where the ordinate is time and abscissa is depth (in m). Black contours mark denote biomass levels of  $175 \text{ mg m}^{-3}$  for Okha and Kanyakumari, and  $215 \text{ mg m}^{-3}$  for the remaining other locations. These thresholds contours are location-specific, and best capture seasonality based on were chosen to optimally represent seasonal biomass variation in relation to local physico-chemical conditions. The top  $\sim 10\%$  of backscatter data is, and hence the biomass data, were excluded due to echo-induced noise. The A dashed horizontal line at 22 m marks the top edge of the first ADCP bin (i.e., centered at 24 m). Vertical black lines separate yearsmark year boundaries, while horizontal black and blue lines indicate represent 40 m and 104 m depths, respectively. Off At Kollam in 2020, no consistent strong year-to-year variation prevents assignment of a distinctive biomass demarcating contour is shown due as compared to strong interannual variabilityother years of the same location.

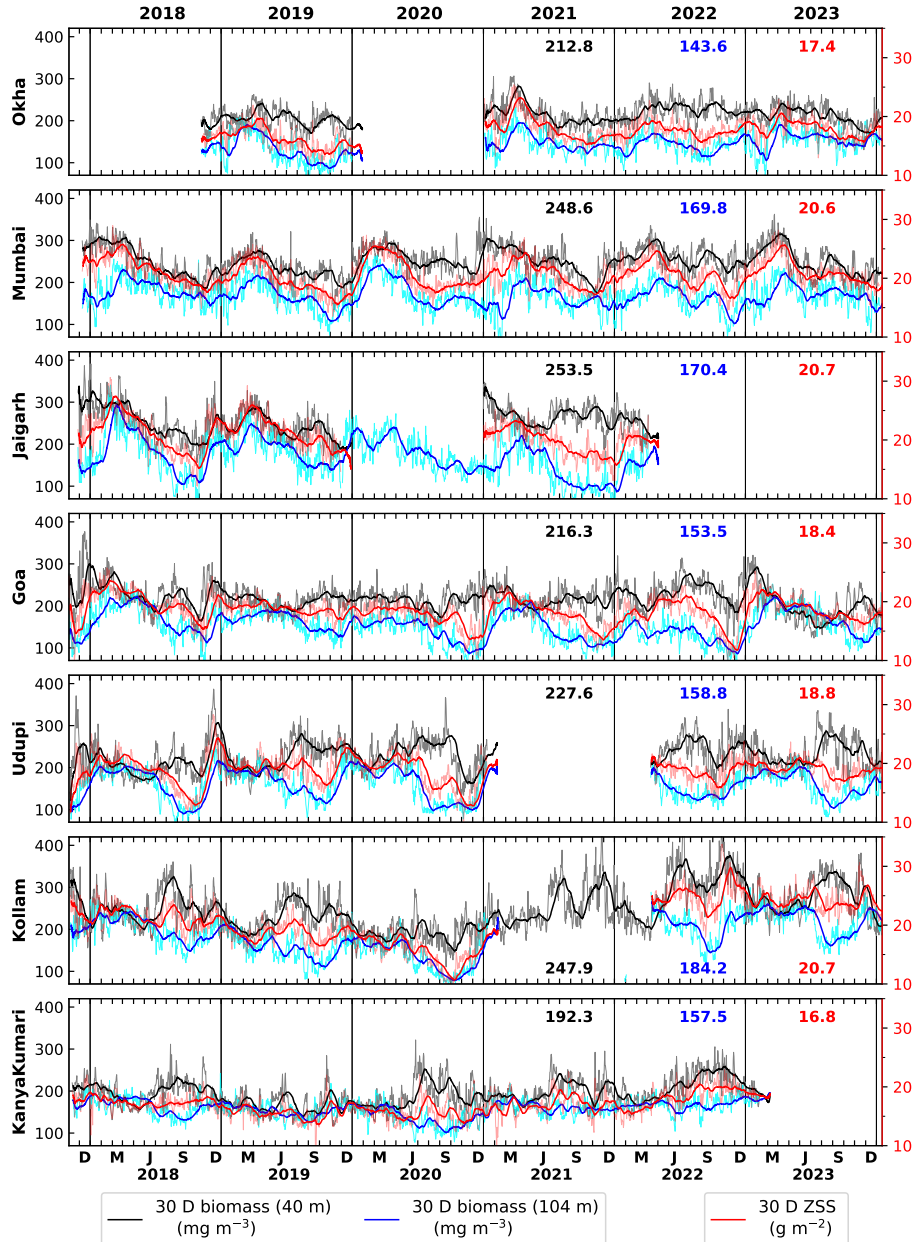


**Figure 4:** Biomass at 40 m (grey and black) and 104 m (cyan and blue), along with ZSS zooplankton standing stock (ZSS; pink and red; integrated over 24–120 m), are shown with where lighter shades representing daily values and darker shades indicating 30-day rolling averages. Mean The biomass time series at 40 m and 104 m share a common ordinate, labeled on the left axis with units  $\text{mg m}^{-3}$ , whereas the ZSS time series uses a separate ordinate displayed on the right with units  $\text{gm m}^{-2}$ . The mean biomass at 40 m and 104 m, as well as the mean ZSS, are noted in the top-right corner in corresponding colors using their respective color codes. Spikes Short-lived biomass spikes (bursts appearing in the daily data) and longer-duration bursts (visible in biomass the rolling mean) are evident, e.g., at 40 m appear in the daily spikes (rolling mean bursts) data, typically lasting a few days (or several days to weeks), e.g., during isolated days in June 2020 (or throughout June–July 2020) off the SEAS. Similar features are observed at all locations at both depths 104 m also, though with varying magnitudes magnitude.

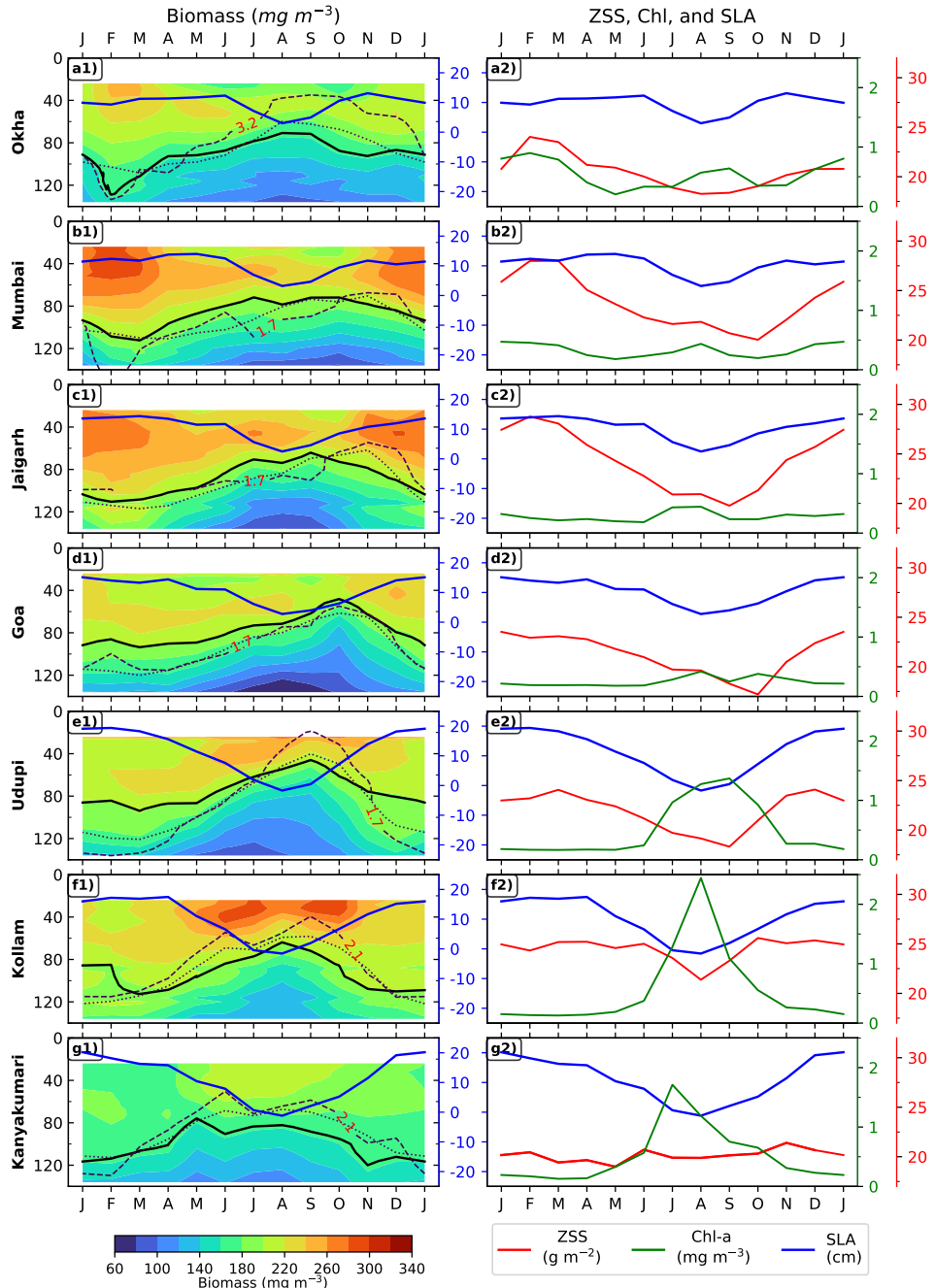


**Figure 5:** Monthly climatology of zooplankton biomass and environmental parameters at seven mooring locations. The left panels show the monthly climatology of zooplankton biomass ( $\text{mg m}^{-3}$ ) for each location. The right panels present the climatology of ZSS (biomass integrated over 24–140 m, derived from the climatology) and chl-a (mg  $\text{m}^{-3}$ ) for each site. The solid blue line indicates the corresponding locations overlaid onto climatological sea level anomaly (SLA), computed from data spanning October 2017 to December 2023. The ordinate and labels are color-coded for clarity.

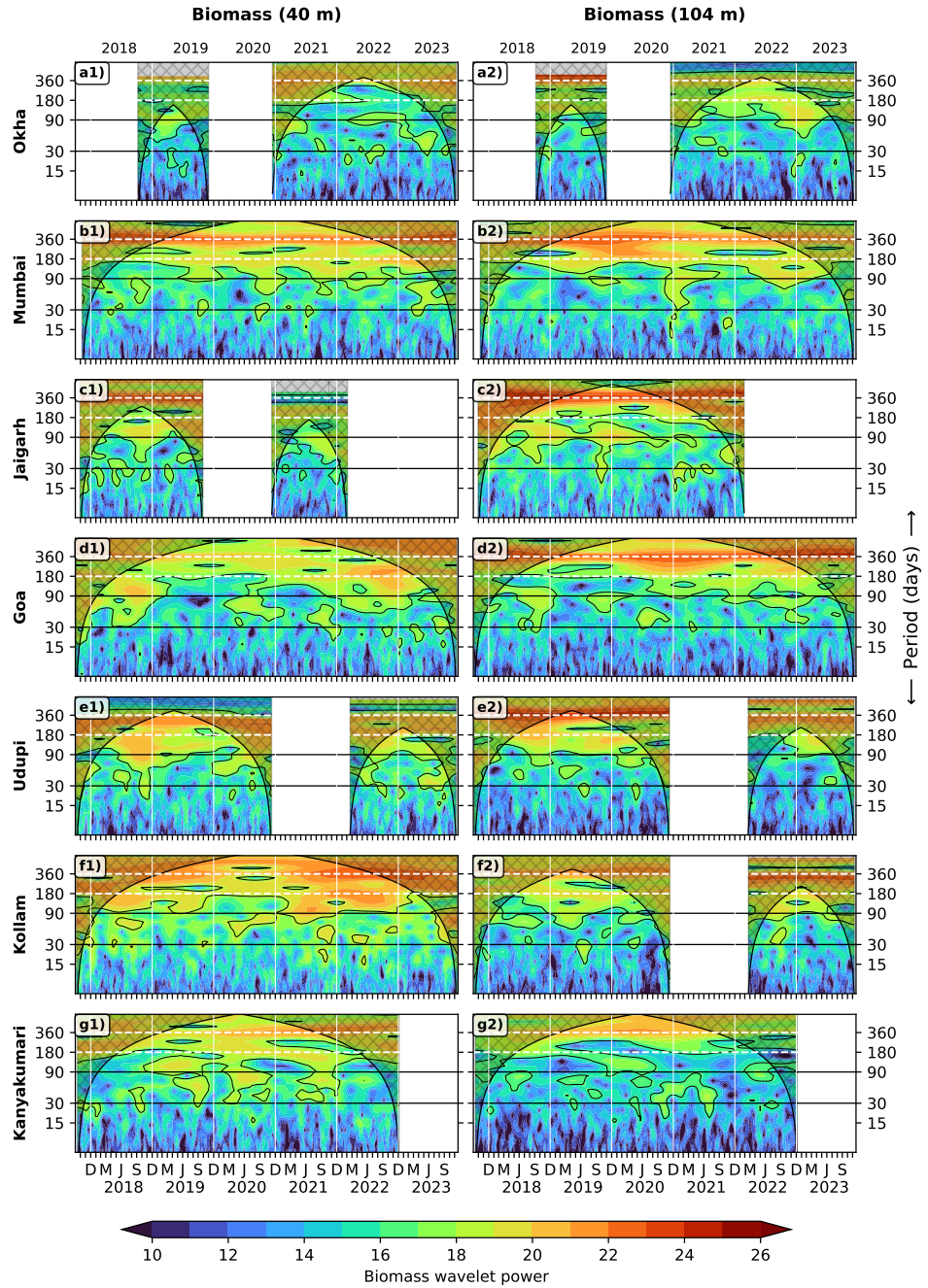


**Figure 6:** Wavelet power spectra (Morlet) of zooplankton biomass at 40 m (left panels) and 104 m (right panels), with time on for seven mooring locations in the eastern Arabian Sea, arranged from north to south. The x-axis shows time, and the y-axis shows period (in days) on the y-axis. Power (Wavelet power and period) is shown represented on a log<sub>2</sub>-log<sub>2</sub> scale. The 95% significance level is outlined by black contours, and the cross-hatched region indicates solid black line marks the cone of influence, delineating the semi-transparent shaded region where edge effects become significant and power values are considered unreliable. Horizontal dashed white and solid black lines mark the annual and semi-annual periods, and solid black lines contain intraseasonal bands, respectively (band 30–90 days). Vertical white lines separate years denote calendar year boundaries. High-power regions indicate dominant temporal scales of biomass variability across depths and sub-regions of the EAS.

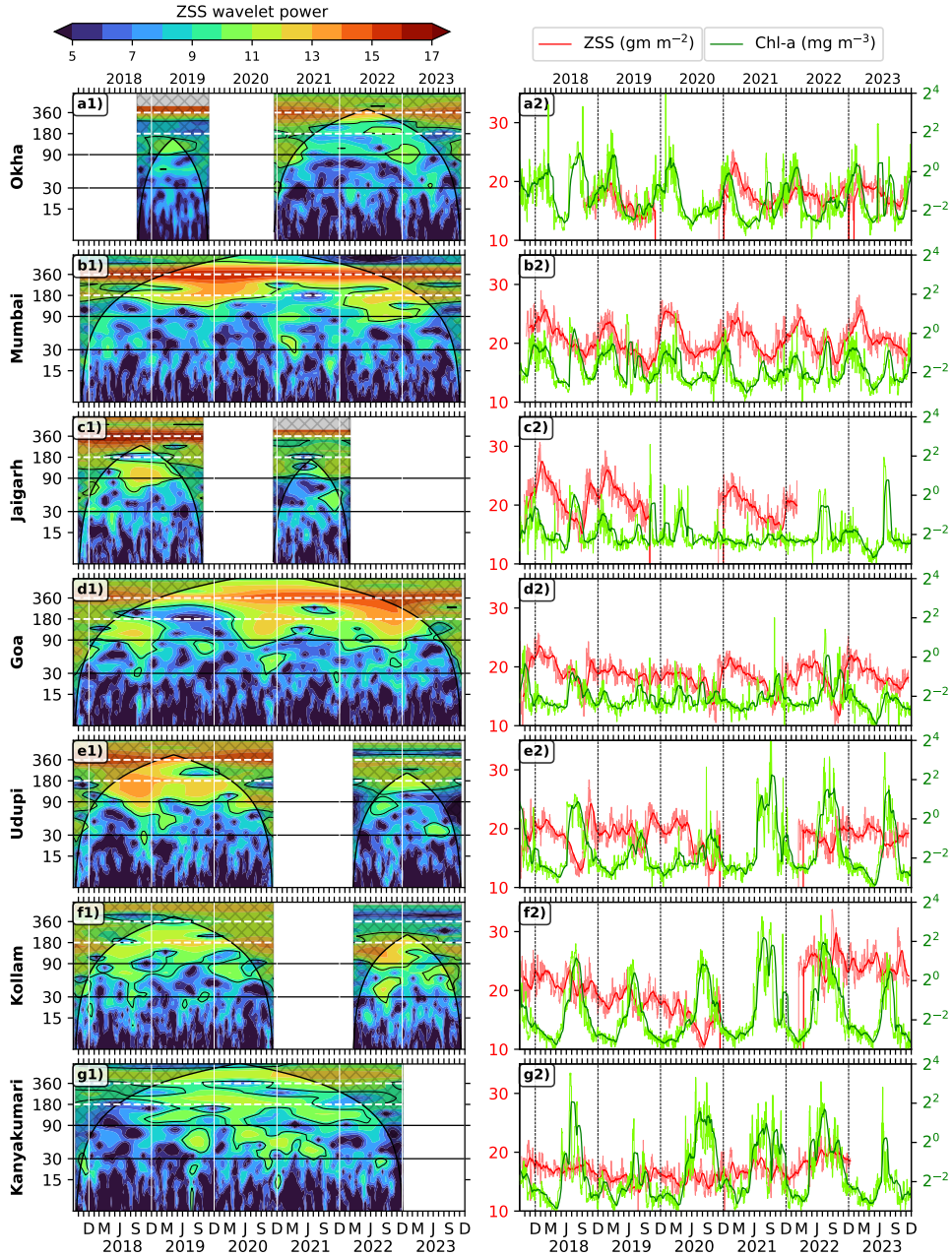


**Figure 7:** The left panel shows the wavelet power spectra (Morlet) of ZSS are shown in the left panel, with time on the x-axis and period (in days) on the y-axis. Power is displayed on a  $\log_2$ - $\log_2$  scale, and regions exceeding the 95% significance level are outlined in black contours, and the solid black line marks the cone of influence, delineating the semi-transparent shaded region where power values are considered unreliable due to edge effects. Horizontal dashed white line mark annual and semi-annual periods, and solid black lines contain intraseasonal band (30–90 days). Vertical white lines separate years denote year boundaries. The right panel shows presents the time series of ZSS (biomass integrated over 24–120 m biomass integral) time series, with the daily values in pink and a 30-day rolling mean (in red) overlaid on daily values (pink). Similarly, the 30-day The rolling mean of chl-a (is overlaid in solid green) is plotted over with its daily values (shown in light green). Rolling means for chl-a and ZSS averages are computed only when at least 10 and 25 valid data points, respectively, ZSS values and 10 valid chl-a values are available within the 30-day window. The higher power in the annual period off Mumbai and Goa in annual band coincides with the annual band.

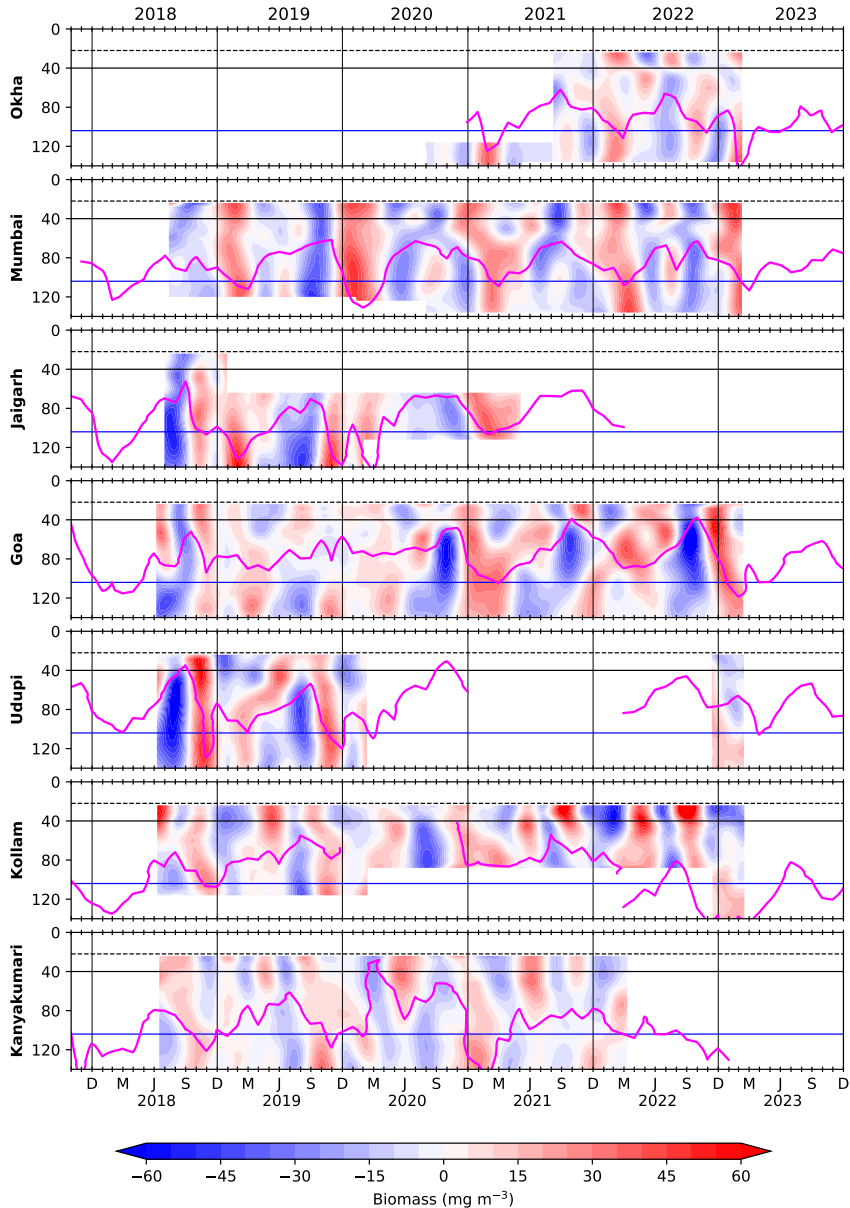


**Figure 8:** Biomass variation variability in the combined seasonal band (100–400 days). The seasonal cycle includes band comprises: (1) annual variation driven by associated with upwelling (downwelling) during the summer (monsoon and downwelling during the winter monsoon), and (2) intra-annual variation due to variability driven by seasonal asymmetry. Horizontal black and blue lines indicate depths of 40 m and 104 m depths, respectively; vertical grey lines separate calendar years. The dashed line at 22 m marks the upper edge of the first ADCP bin (i.e., centered at 24 m). Solid magenta curves represent D215 (D175–D175 off Okha and Kanyakumari), derived from monthly biomass data climatology.

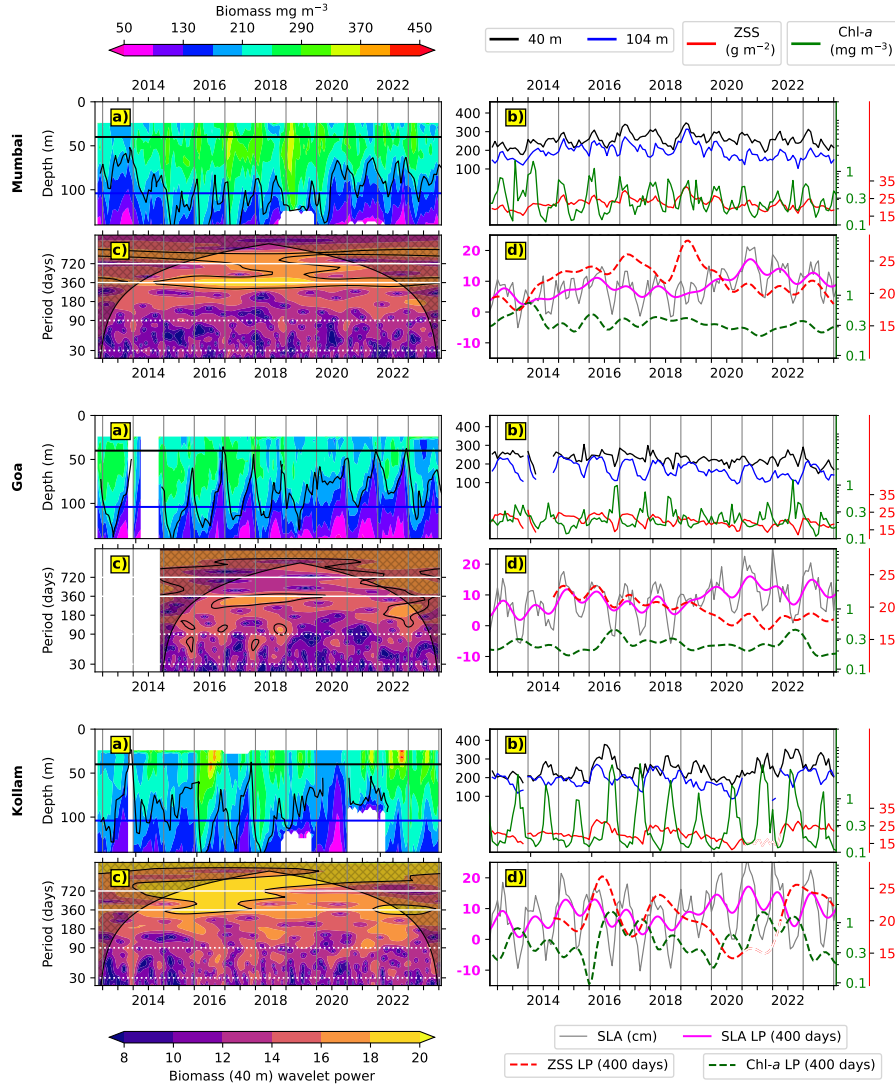


**Figure 9:** Decade-long biomass records off from Mumbai, Goa, and Kollam are shown in the left. Each location is represented by a set of four panels. The top four panels correspond to Mumbai: (a) Time vs depth figure of biomass, with black and blue lines indicating biomass at 40 m and 104 m, respectively; vertical grey lines separate years. Biomass is in units  $\text{mg m}^{-3}$ . Below each record (black) and 104 m (blue), wavelet overlaid with ZSS (red) and chl-a (green). (c) Wavelet power spectra of 40 m biomass are shown, with dashed white lines marking periodicities 720 and 360 days, and dotted lines delineate the intraseasonal band (30–90 days). The right panels show time series of biomass at 40 m (black) and 104 m. Monthly resampled SLA (bluegrey), alongside ZSS overlaid with its 400-day low-pass filtered signal (redmagenta) and. Also shown are the 400-day low-pass Butterworth-filtered time series of chl-a (green) for the respective locations and ZSS. All time series variables are resampled to a monthly time axis. Sea level anomaly (SLA, grey) and the units are: biomass (40 m and 104 m) –  $\text{mg m}^{-3}$ ; ZSS –  $\text{g m}^{-2}$ ; chl-a –  $\text{mg m}^{-3}$ ; SLA – cm. The same panel arrangement is shown adjacent to the wavelet panels, overlaid with its 300-day low-pass filtered signal repeated for Goa (magenta middle set) and Kollam (bottom set). A clear biennial signal is observed off Kollam, appears weaker off Goa, but becomes more evident again off Mumbai.

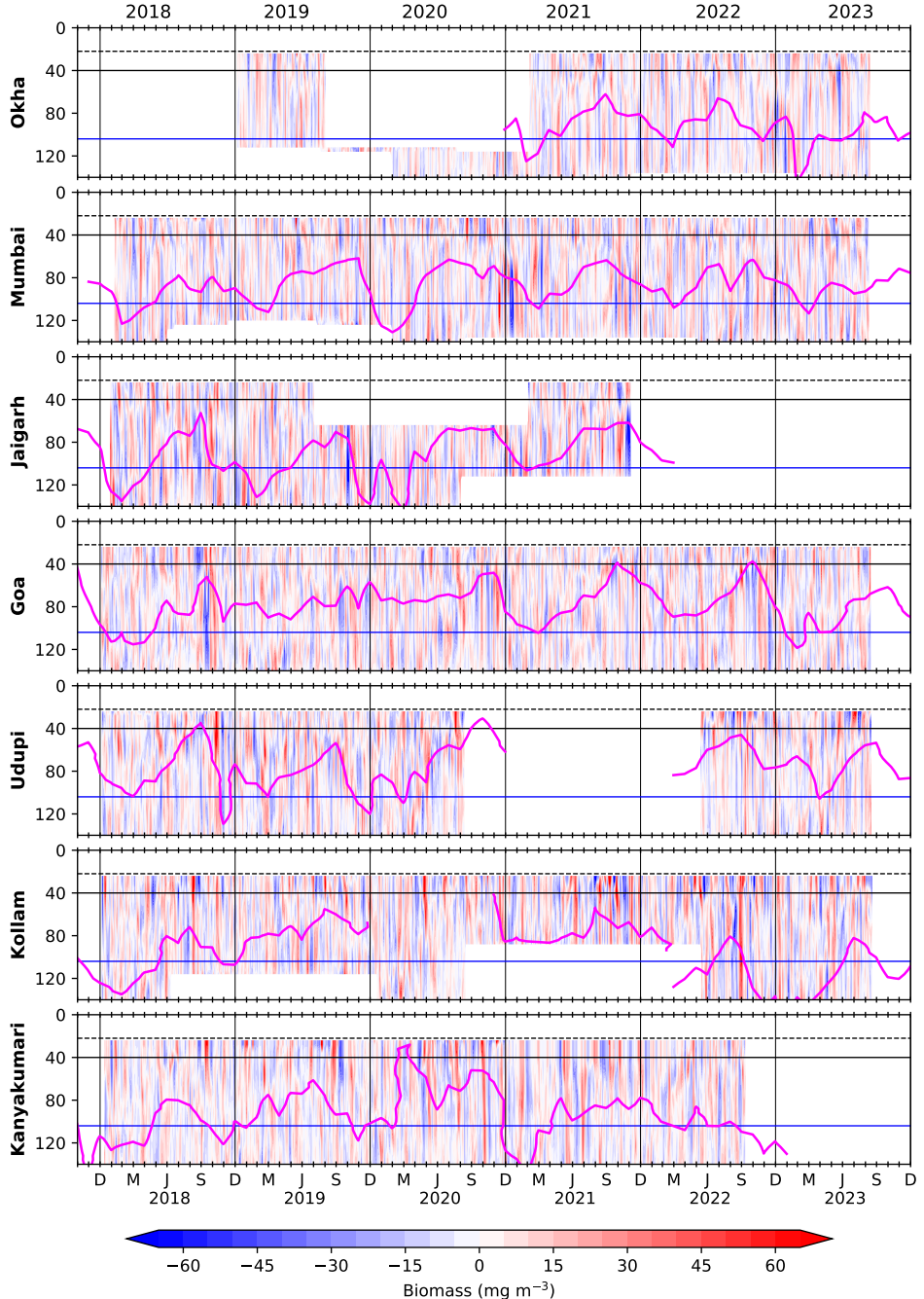


**Figure 10:** Biomass variation in the intraseasonal band (5–90 day period) is extracted using a Lanczos band-pass filter, capturing both high- and low-frequency intraseasonal components. Horizontal black and blue lines represent depths of 40 m and 104 m, respectively. Vertical black lines separate calendar years, and solid magenta curves indicate  $D215$  (or  $D175$  off Okha and Kanyakumari), derived from monthly biomass. The dashed line at 22 m marks the upper boundary of the first bin (centered at 24 m). Intraseasonal variability is evident throughout the time series and appears coherent along the slope, notably during October–December 2018.

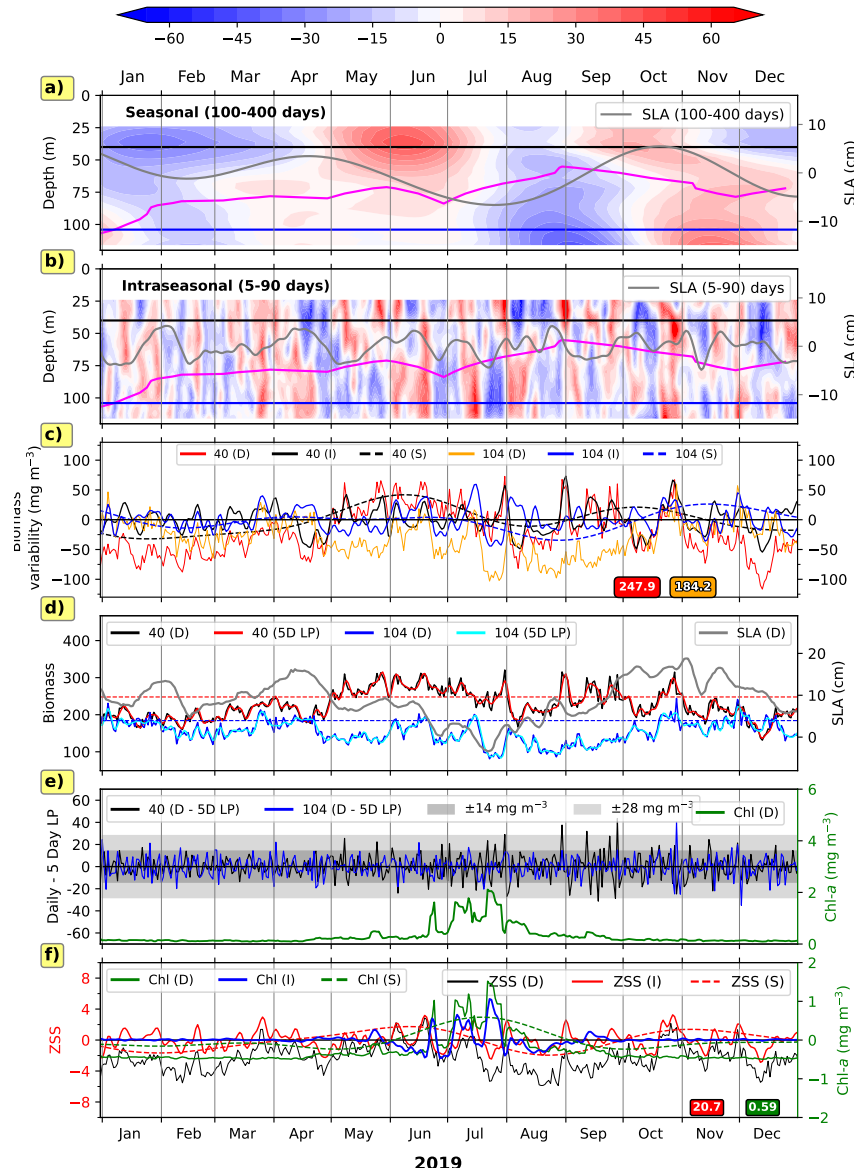


**Figure 11:** The figure shows a comparison of biomass variability ( $\text{mg m}^{-3}$ ) in the seasonal (100–400 days) and intraseasonal (5–90 days) bands off Kollam. The top two panels display time–depth plots of seasonal and intraseasonal biomass on the same color scale, respectively. D215 is marked in magenta. Overlaid grey contours represent the corresponding SLA. Biomass at 40 m and 104 m are marked by black and blue horizontal lines, respectively, and vertical grey lines indicate month boundaries. The third panel from the top shows the daily, intraseasonal, and seasonal biomass at 40 m and 104 m, along with its intraseasonal (5–90 days) and seasonal (100–400 days) components. The mean of the daily biomass time series for each depth 40 m (red) and 104 m (orange) is noted in the bottom right corner of the panel. The fourth panel presents daily biomass overlaid with its 5-day low-pass filtered version and the daily sea level anomaly (SLA). Panels (a) and (b) compare daily SLA with daily and 5-day low-pass filtered biomass at 40 m and 104 m. Panel (c) illustrates the difference between daily and 5-day low-pass filtered biomass at 40 m and 104 m; grey both depths. Grey and light grey shaded regions indicate the  $\pm 1$  standard deviation ( $\pm 1$  SD) and  $\pm 2$  SD envelopes of the backscatter-to-biomass relationship, respectively, over which daily derived